GEOLOGICAL SURVEY OF CANADA
OPEN FILE 8110

The ups and downs of the Canadian Shield: 1- preliminary results of apatite fission track analysis from Hudson Bay region

N. Pinet, B. P. Kohn and D. Lavoie

2016

Celebrating 175 yrs

The ups and downs of the Canadian Shield: 1- preliminary results of apatite fission track analysis from Hudson Bay region

N. Pinet[1], B. P. Kohn[2] and D. Lavoie[1]

[1] Geological Survey of Canada, 490 de la Couronne, Québec, Quebec G1K 9A9

[2] School of Earth Sciences, University of Melbourne, Australia

2016

Publications in this series have not been edited; they are released as submitted by the author.

The ups and downs of the Canadian Shield: 1- preliminary results of apatite fission track analysis from the Hudson Bay region.

Nicolas Pinet [1], Barry, P. Kohn [2] and Denis Lavoie [1]

[1] Natural Resources Canada, Geological Survey of Canada, 490 rue de la Couronne, Québec, Quebec, G1K 9A9

[2] School of Earth Sciences, University of Melbourne, Melbourne, Victoria 3010, Australia.

Abstract: The low-temperature (120-60°C) thermal history of seven samples from the Hudson Bay region has been investigated using apatite fission-track (AFT) analysis. Apatite grains from six Precambrian rock samples from the surface or the bottom of hydrocarbon-targeted wells and from one sample belonging to a thin Upper Ordovician sandstone unit at the base of the Paleozoic succession were analysed. All apatite fission-track (AFT) ages are younger than the age of their host rocks indicating that fission tracks experienced significant post-crystallisation or deposition annealing and samples were subjected to temperatures > 60°C. The track length distributions suggest slow cooling. AFT pooled ages range from 215.1 ± 15.0 to 462.7 ± 29.9 Ma. The sample from Akpatok Island, in Hudson Strait has the youngest AFT age, suggesting that the exhumation history of this area may be different from the Hudson Bay Basin.

Inverse modeling of AFT data provides an estimate of the maximum temperature experienced during the Paleozoic burial episode and, with much less accuracy, the timing of maximum heating. For the two wells that have both organic matter maturation and AFT data, the measured vitrinite equivalent value is higher than that calculated reflectance using AFT inverse modeling results. AFT results from the Hudson Bay region are broadly in agreement with those reported for the southern Canadian Shield. However, the available dataset is not sufficient to depict regional variations of maximum heating conditions, an issue that is critical for the hydrocarbon assessment of the area.

Introduction

The Canadian Shield is an iconic example of a cratonic area characterized by an old (> 1 Ga), thick (ca. 240-280 km thick beneath Hudson Bay), cold and stiff lithosphere (Eaton and Darbyshire, 2009). Like most continental interiors, the Canadian Shield is considered relatively stable, and most geological models infer a slow and more or less continuous exhumation punctuated by relatively minor sedimentary or ice-sheet loading events. However, several lines of evidence imply that younger sedimentary units have been deposited and subsequently eroded away from vast areas. Quantification of the thickness, age and geographical distribution of the missing geological record is not an easy task, but has major implications for the geological history and hydrocarbon prospectivity of intracratonic basins.

Paleozoic sedimentary xenoliths found in kimberlite pipes of the Canadian Shield provide direct evidence for a now eroded sedimentary cover. Such xenoliths have been documented in Northwest Territories (Slave Craton, Middle Devonian xenoliths; Cookenboo et al., 1998), in Ontario (Kirkland Lake area; Ordovician to Devonian xenoliths; McCracken et al., 2000) and in Nunavut (Baffin Island; Late Ordovician-early Silurian xenoliths; Zhang and Pell, 2014). In the Hudson Bay intracratonic basin, organic maturation data (Reyes et al., 2011; Bertrand and Malo, 2012) shows that preserved sediments alone cannot explain the suggested maximum burial conditions; either a significant part of the succession has been removed by erosion and/or high geothermal gradients prevailed in the past (Pinet et al., 2013). Apatite fission track (AFT) analysis is an independent method that may constrain the thermal history at relatively low-temperatures (typically < 120°C). Here we report AFT data for seven samples from the Hudson Bay region and provide preliminary interpretations. Another aim of this open file is to discuss modeling strategies and scenarios in more detail than is usually possible in scientific journals.

1. Geological background

In central Canada, the Phanerozoic sedimentary succession preserved in Hudson Bay Basin (Fig. 1) unconformably overlies the Precambrian Canadian Shield, which includes metamorphic and igneous rocks belonging to a number of lithospheric blocks that amalgamated during the Archean to Paleoproterozoic (Eaton and Darbyshire, 2009). This sedimentary succession is up to 2500 m thick and was deposited under shallow marine conditions (Lavoie et al., 2015). The basin has a relatively simple geometry, characterized by an Upper Ordovician to Lower Devonian sedimentary package that is cut by high-angle faults and overlain by a saucer-shaped, essentially undeformed, Middle to Upper Devonian sedimentary package (Pinet et al., 2013). The main structural

feature is a NNW trending composite central high that extends for a minimum length of 500 km, the origin of which is likely linked to far-field orogenic events at the Laurentian continental margin (Pinet, 2016).

Paleozoic strata are unconformably overlain by thin, discontinuous erosional remnants of Jurassic, Cretaceous and mid-Cenozoic non marine and marine strata (Lavoie et al., 2013).
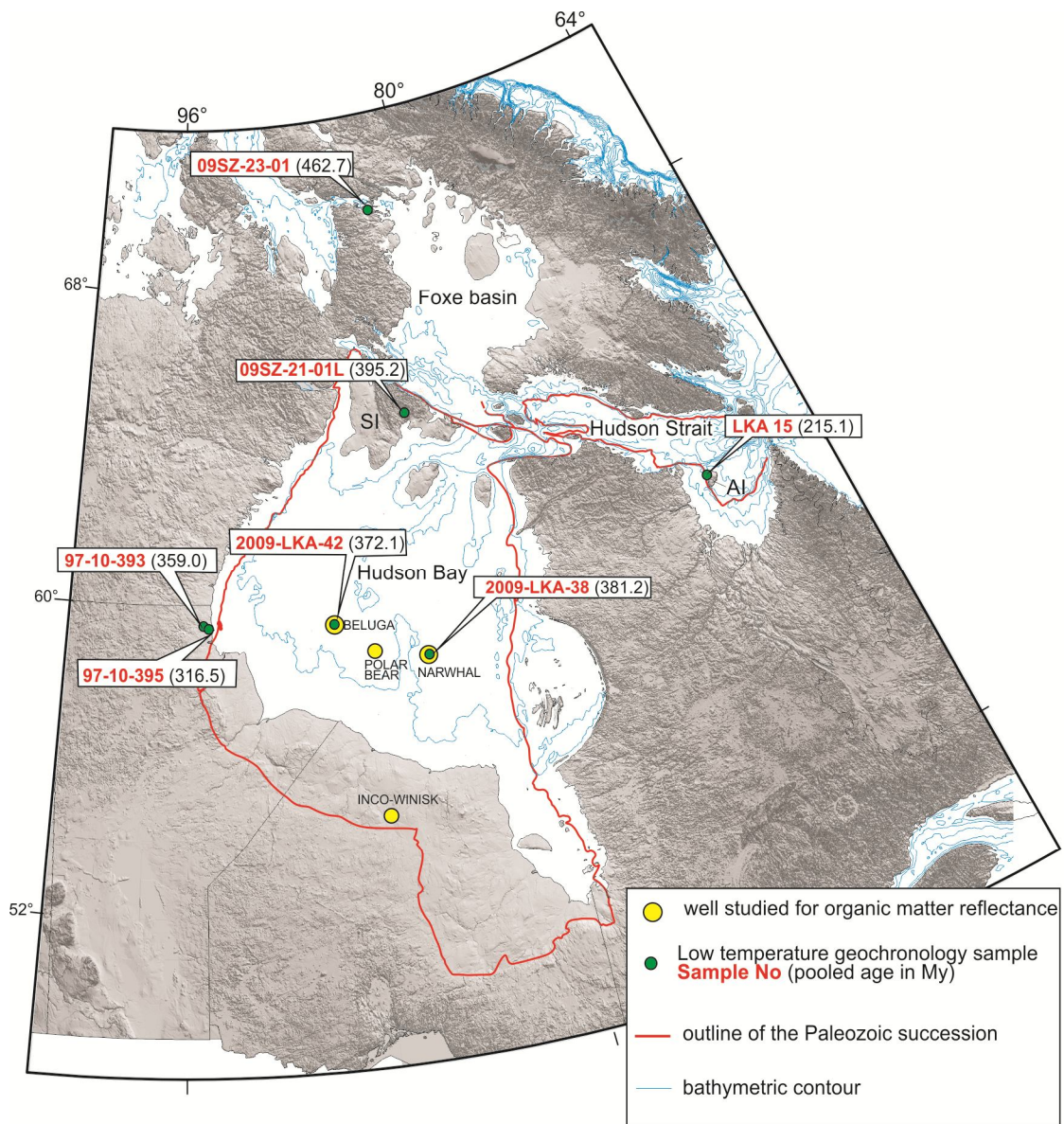

Figure 1: Location of samples studied (modified from Lavoie et al., 2015). AI, Akpatok Island; SI, Southampton Island.

2. The apatite fission track method

Apatite fission-track (AFT) analysis has been widely used during the past decades to constrain the low-temperature thermal histories of many areas around the world, in different geological settings. Isotopic dating methods are based on the ratio of parent and daughter isotopes, although for AFT analysis the daughter product is not another isotope but rather a trail of physical damage to the crystal lattice resulting from spontaneous fission of ^{238}U.

Fission tracks form at similar initial lengths continuously over time, at a rate dependent upon only uranium concentration. The fission tracks are shortened in the partial annealing zone (PAZ) that corresponds to temperatures between ~60°C and ~110°C (up to 130-140°C for the most 'resistant' apatite). This partial annealing temperature range includes most of what is known as the oil window for organic matter thermal maturation; hence AFT analyses provide useful information with respect to hydrocarbon generation in sedimentary basins (Osadetz et al., 2002; Green and Duddy, 2012). At lower temperatures than the PAZ, fission tracks are still shortened but at much lower rates, whereas at higher temperatures, tracks are completely erased (annealed). During exhumation, earlier-formed tracks will tend to be shorter than later-formed ones, as they will have more time to anneal and may have experienced higher temperatures. The change in length of AFT varies among apatite crystals and two proxies are commonly used to estimate the kinetics of the annealing process: Dpar, which is a measure of the long axis of the etch pit opening (in µm) parallel to the crystallographic c-axis and the chlorine content (in weight %).

Interpretation of AFT data is based on the combined analysis of the fission track age, track length distribution and a kinetic parameter. Fission track ages do not usually indicate the timing of cooling through a specific temperature (except for nearly instantaneous cooling, such as in volcanic settings), but instead represent the integrated thermal history of studied samples. Excellent reviews on the AFT method are found in Gallagher et al. (1998), Gleadow et al. (2002), Donelick et al. (2005), Ketcham (2005) and Green and Duddy (2012).

3. Forward models of simple thermal histories

Forward modelling tools allow calculation of the age and track length distribution that should be observed for a particular thermal history and set of kinetic parameters. In other words, forward models illustrate the effects of time-temperature history and kinetic variability on AFT results. They provide a simple way to test simple thermal histories and maybe more importantly, illustrate which information is not contained in AFT results.

In the area surrounding the Hudson Bay Basin, the post Paleo-Proterozoic geological history can be divided into three main stages: 1) a period of regional exhumation

following the Trans-Hudson orogeny; 2) a period of burial from the Late Ordovician to the Late Devonian or later; 3) a second period of regional exhumation following Paleozoic sedimentation. In Figures 2 and 3, this basic geological history is investigated in order to illustrate the variable influence of some parameters on AFT results.

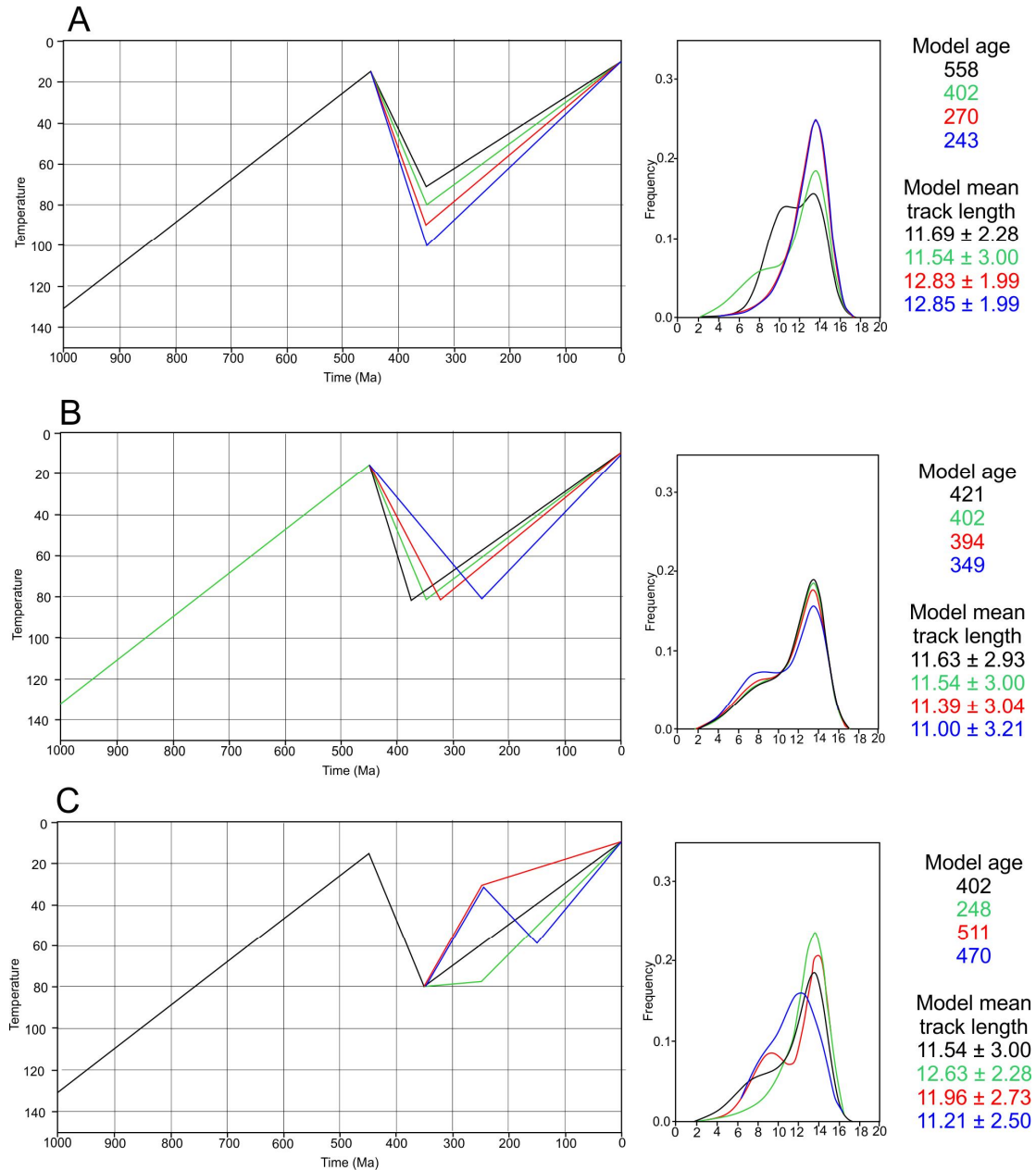Figure 2: Forward models illustrating the influence of: (A) the maximum temperature (B) the timing of maximum temperature and (C) the exhumation path on AFT parameters (age and length distribution). Various scenarios are indicated by different colors on the time-temperature diagrams to the left of the figure. The same colors applied for the calculated fission track length distribution and to model results in right hand panels.

In the four scenarios presented in Figure 2A, the maximum burial occurred at 350 Ma, but the maximum temperature varies between 70°C and 100°C. Depending of the scenario, the model age varies significantly, but most importantly the track length distribution differs markedly. A bimodal distribution characterizes lower temperature scenarios as short tracks associated with the pre-Ordovician history were not significantly annealed and a slightly skewed unimodal distribution is associated with higher temperature scenarios. This highlights the fact that if appropriate kinematic parameters are used, maximum temperature can be confidently resolved with AFT analysis.

Figure 2B presents four scenarios in which the post-Ordovician maximum paleotemperature (80°C; similar to the maximum temperature indicated by the data presented here, see below) is reached at a variety of times, between 380 Ma and 250 Ma. Model age and model mean fission track length vary only moderately, and the track length distribution is almost identical in all scenarios. This indicates that the timing of maximum burial may be challenging to constrain in the case of slow exhumation and maximum temperatures near the lower temperature limit of the PAZ, as might be expected for the Hudson Bay region.

Figure 2C shows that variations in the time-temperature path during post-Ordovician exhumation moderately influence the model age and model average track length, excepted when a scenario with a long residence period close to the maximum paleo-temperature is considered (green path on Figure 2C). In this last case, the model age is much younger, the model average track length much longer than for other scenarios, and the track length distribution is negatively skewed and unimodal.

Figure 3 investigates the influence of the pre-Ordovician thermal history on AFT analysis. The five scenarios presented in Figure 3A start at 1 Ga but at temperatures varying between 90°C and 150°C. Model age and model average track length are only slightly different indicating that the pre-Ordovician history is poorly resolved. Moreover, a time-temperature path involving a more complex thermal history (pink path on Figure 3A) is indistinguishable from other scenarios.

In Figure 3B, the three forward models start at a temperature of 130°C, and between 2.0 to 1.0 Ga, implying various, but lengthy periods of residence in the PAZ. Model ages and model average lengths are significantly different, but the length distribution for the three scenarios diverges mainly in the shorter track length range, which is usually poorly defined from an analytical point of view. This indicates that the pre-Ordovician history has some influence on AFT results, especially if subsequent burial was moderate (in the upper part of the apatite PAZ).
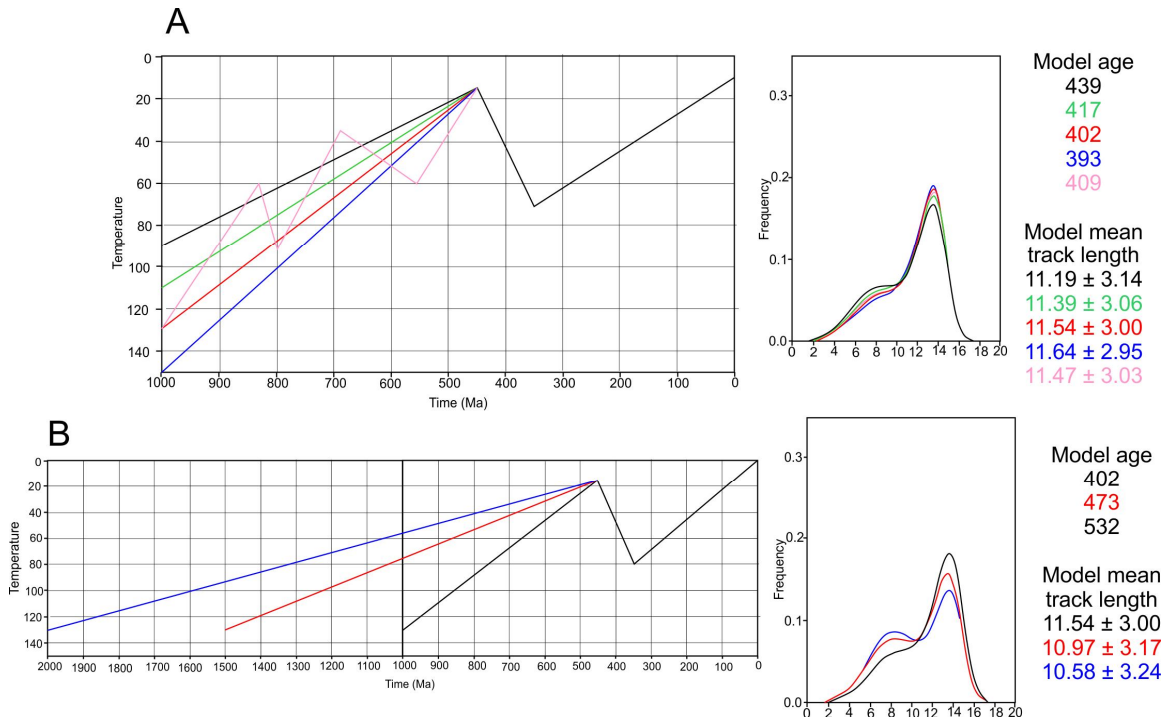
Figure 3: Forward models illustrating the influence of: (A) the temperature at the beginning of the models (1 Ga) and (B) the initial time on AFT ages and length distributions. Various scenarios are indicated by different colors on the time-temperature panels to the left. The same colors applied for the calculated fission track length distribution and to model results shown in the right hand panels.

4. Data

4a. Methodology

The AFT analyses reported here were conducted at the University of Melbourne (Australia). Seven samples were first analysed in 2013. For the same samples, analyses of different apatite grains from the same mounts were conducted in 2016 to take advantage of recent improvements in methodology.

All rock samples were broken into small pieces using a hydraulic splitter and jaw crusher, then ground in a disc mill and sieved to fragments <500 μm. The sieved material was then run over a Wifley mineral separation table to produce an initial heavy mineral concentrate, which was then treated with conventional magnetic and heavy liquid techniques to produce an apatite-bearing fraction.

Apatite grains were mounted in epoxy resin on glass slides, ground and polished to an optical finish using diamond paste to expose internal grain surfaces. Polished mounts were etched in 5M HNO_3 for 20 seconds at 21°C to reveal the fossil tracks. In 2013, an aluminium coating with a 5-7 nm thickness was applied to the etched mounts to

enhance the reflectivity of the polished surface, and minimize internal reflections (Gleadow et al, 2009). Analysis done in 2016 used an Au coating. Apatite grains with polished surfaces parallel to prismatic crystal faces and relatively homogeneous track distributions were selected for analysis using recent developments in digital microscopy, image analysis and computer software (designed for capturing high resolution images) which provide opportunities for a new automated counting approach for apatite fission-track analysis (e.g., Gleadow et al., 2015).

For this work, software (*TrackWorks*[©] and *FastTracks*[©]) recently developed by the Thermochronology Group at the University of Melbourne and Autoscan Systems were used. This software suite controls a Zeiss M1 digital microscope fitted with a high-resolution camera and an AutoScan[©] stage and is used at a total magnification of x1000 under both transmitted and reflected light for capturing images of the apatite crystals for determining the spontaneous track density on the crystals. The advantage of this procedure is that a permanent digital record of analysed crystals is stored and is available for later inspection, even after grains have been partly destroyed by laser ablation at a later stage. Further, this protocol offers improved accuracy for measuring the areas over which spontaneous tracks are counted as well as the visualization of crystals on a computer monitor.

Uranium content of the grains on which spontaneous track counts had been made was determined by LA-ICP-MS (Inductively Coupled Plasma Mass Spectrometry) single spot analysis on the same grains on which spontaneous fission tracks had been counted, using a New Wave Nd:YAG Laser (λ = 213 nm with 5Hz @ 45% power, spot size µm) connected to an Agilent 7700 mass spectrometer. NIST612 was used as an internal LA-ICP-MS standard.

Fully etched confined track length and etch pit diameters (Dpar) of grains, were also measured from digital images after the *c*-axis had been determined using *FastTracks*[©] on polished surfaces parallel to prismatic crystal faces. Digital magnification that can be generated from the high-resolution images and the measuring tools in this software enables the user to determine the confined fission track lengths and Dpars with improved accuracy.

4b. Results

Apatite fission track (AFT) results for seven samples (six from crystalline basement and one from sediment) are summarized in Tables 1 and 2, and correspond to analyses carried out in 2016.

Three revised (2016) ages overlap ages reported in Lavoie et al. (2013) when the ± 2 sigma age uncertainties are considered. Three of the revised ages are older than the original ages, and one is younger.

The difference in AFT ages based on 2013 analyses and those based on 2016 analyses probably results from the interplay of three main factors: 1) a slight change in the zeta value, a parameter that includes several experimental terms (see below); 2) a variation in track revelation efficiency under automation due to the change in coating on grain mounts from Al to Au; 3) a slight change in LA-ICP-MS conditions in terms of laser settings and standards used.

For most samples, grain quality was good to excellent, allowing for age determinations based on 14-23 apatite grains per samples in 2016, measurement of up to 101 horizontal confined track lengths and 152 Dpar measurements.

Sample No.	Lithology	Age	Location	Latitude °N	Longitude °W	Depth or elevation (m)	Apatite yield
Sediments							
09SZ-21-01L	Paleozoic Sandstone	Ord	Southampton Island	64.284694	-83.10660	150	excellent
Crystallines							
09SZ-23-01	Granite	PreCamb	Melville	69.4966	-82.84220	15	excellent
2009-LKA-15+16+17	Gneiss	PreCamb	Akpatok F-26	60.424606	-68.33575	-365	excellent
2009-LKA-38	Gneiss	PreCamb	Narwhal South O-58	58.133442	-84.134053	-1310	good
2009-LKA-42	Gneiss	PreCamb	Beluga O-23	59.215175	-88.557453	-2200	good
97-10-395	K-spar porphyritic hblde-bi-granite	PreCamb	Outcrop - Manitoba	59.34891	-95.04501	35	excellent
97-10-393	K-spar porphyritic hblde-bi-granite	PreCamb	Outcrop - Manitoba	59.302684	-94.81463	10	excellent

Table 1: Summary of samples studied for AFT analysis.

The chi-square (χ^2) test calculated for each sample analysed (Table 2) is a standard test for the homogeneity of single grain ages. It provides an assessment of whether the fission track counts were derived from a Poissonian distribution with a common mean value. If the χ^2-statistic $P(\chi^2)$ is ≥ 5%, (as is the case for all samples discussed here) it can be taken as evidence that all grains counted derive from a single age population. In this case, it is appropriate to use the pooled AFT age, rather than the central age (also shown in Table 2), which is a weighted-mean of the log normal distribution of single grain ages (Galbraith and Laslett, 1993).

All samples show a broad horizontal confined track length distribution, with sample 97-10-393 showing a distinctly negatively skewed distribution, due to a tail of shorter track lengths.

All samples exhibit narrow etch pits, suggesting that the predominant composition of the grains analysed is fluorapatite. This was confirmed by electron microprobe analyses of apatites. Average Cl wt% of apatite on which ATF ages were originally determined in 2013 ranges from 0.01 to 0.14% (maximum single grain apatite Cl wt% = 0.32). Apatite grains with such low values of Cl wt% usually anneal more readily relative to those with higher Cl wt% (> 1-2%), (Donelick et al., 2005).

Crystalline basement rocks yield AFT pooled ages ranging from 215.1 ± 15.0 to 462.7 ± 29.9 Ma. The oldest AFT age is from the Melville Peninsula, close to the Foxe Basin western margin (Fig. 1). The youngest AFT age is from a sample at the bottom of the Aktapok well, which is the closest to the Atlantic margin (Hudson Strait, Fig. 1). The single sedimentary sample (09SZ-21-01L) analysed from an Ordovician sandstone outcrop on Southampton Island, yields an AFT age of 395.2 ± 24.5 Ma. All AFT ages are substantially younger than the metamorphic/magmatic or deposition age of their host rocks.

Sample No.	No. of grains	N_s	ρ_s [10^5 cm^{-2}]	^{238}U [ppm ± 1σ]	P(χ2) (%)	Dispersion (%)	Pooled age [Ma ± 1σ]	Central age [Ma ± 1σ]
LKA-15	15	1401	1,29E+06	11.68 ± 12.14	13,58	17	215,1 ± 15,0	230,6 ± 13,5
LKA-38	22	2877	3,56E+06	17.93 ± 6.33	49,82	16	381,2 ± 16,5	377,1 ± 15,5
LKA-42	21	1454	1,51E+06	8.1 ± 5.27	52,79	23	372,1 ± 23,8	372,2 ± 22,5
09SZ-21-01L	15	1229	3,24E+06	16.75 ± 12.15	44,4	18	395,2 ± 24,5	393,0 ± 23,0
09SZ-23-01	19	1921	1,41E+06	5.69 ± 2.67	31,05	21	462,7 ± 29,9	485,5 ± 26,7
393	23	4270	3,67E+06	19.94 ± 3.8	32,98	12	359,0 ± 12,1	358,6 ± 11,4
395	14	1950	3,04E+06	18.17 ± 7.79	32,5	14	316,5 ± 16,7	324,8 ± 15,6

Table 2: AFT age results for seven samples from the Hudson Bay region.

N_s, number of spontaneous tracks counted
ρ_s, fossil track density
^{238}U, Pooled uranium content of all grains measured by LA-ICP-MS
P(χ2), P value of χ2 for (n-1) degrees of freedom (Galbraith, 2005)
Dispersion, percentage of variation between single grain ages
Pooled age (Ma), calculated from pooled counts and pooled U content of all grains (Hasebe et al., 2004)
Central age, calculated from single grain ages after Galbraith (2005)

Mean horizontal confined track lengths range from 10.37 ± 0.22 to 12.18 ± 0.15 µm for crystalline basement rocks and is 12.36 ± 0.23 µm for the sandstone sample from Southampton Island (Table 3).

Sample No.	No of track length	Mean track length ± 1SD (µm)			D_{par} [µm]	CI wt% range (mean)
LKA-15	51	12.12	±	0.32	1.42 ± 0.16	0.00-0.004 (0.01)
LKA-38	64	11.08	±	0.26	1.66 ± 0.11	0.02-0.27 (0.14)
LKA-42	60	10.37	±	0.22	1.64 ± 0.11	0.00-0.07 (0.04)
09SZ-21-01L	51	12.36	±	0.23	1.56 ± 0.18	0.01-0.30 (0.13)
09SZ-23-01	100	12.18	±	0.15	1.67 ± 0.16	0.02-0.12 (0.05)
393	101	11.95	±	0.18	1.37 ± 0.08	0.00-0.07 (0.02)
395	100	11.81	±	0.18	1.43 ± 0.11	0.00-0.03 (0.01)

Table 3: AFT track length results and kinetic parameters (D_{par} and CI wt%) for seven samples from the Hudson Bay region. D_{par} corresponds to the etch pit diameter. CI wt% reported corresponds to the apatite grains analysed in 2013 which are used as a proxy for apatite grains studied from the same samples in 2016 and clearly demonstrate the predominance of fluorapatite.

The relatively young AFT ages and short mean track lengths of analyzed samples suggest that they have experienced post-depositional annealing at temperature > 60°C.

5. Inverse modelling and preliminary interpretation

5a. Basic parameters used during inverse modeling

A number of software tools that use several approaches to invert fission track data for modeling thermal histories are available. Modeling strategies and applications are discussed in Issler (1996), Willet (1997), Ketcham (2005), Donelick et al. (2005), Ehlers et al. (2005), Gallagher (2012), Ketcham (2013) and Vermeesch and Tian (2014) amongst others.

In this study, AFT ages, track lengths and Dpar measurements of samples were used to determine time-temperature paths using inverse Monte Carlo modeling (HeFTy software, version 1.8.2; Ketcham, 2013; modified from Ketcham, 2005). The Ketcham et al. (2007) multi-compositional annealing model was used, with *c*-axis projected track data. The Dpar kinetic parameter was used to calibrate annealing kinetics and an initial confined track length (calculated according the formula of Carlson et al., 1999). The

standard length reduction is 0.893 in all models. For the analysis reported here, the Zeta factor (a parameter determined by calibration with international standards of known ages) is: 2001.2 ± 1.1.

HeFTy also allows the user to specify regions of time-temperature space through which each path must pass and the complexity of the paths between these regions. During modeling, particular attention was paid to not over constrain the inversion process, and the time-temperature constraints have been broadly defined except for the near surface conditions experienced at the beginning of Paleozoic sedimentation and at present. Time-temperature constraints vary for each sample and will be described in the following section. In HeFTy, the complexity of time-temperature paths is taken into account by three main parameters:

1) The number of times (n) a path segment between two constraints is halved by introducing a new point allowing a change in slope (2^n segments between constraints). Increasing the number of nodes allows a greater complexity to the model.

2) A qualitative measure of the possible changes in the time-temperature path with three modes: 'episodic' in which sudden changes are allowed, 'intermediate' which is less prone to sudden changes and 'gradual' where the temperature changes gradually over time.

3) A maximal heating/cooling rate for each segment.

The choice of these parameters depends on the tectonic setting and on geological knowledge. Considering the intracratonic setting of the Hudson Bay region, rapid temperature changes are unlikely. Even during the main sedimentation phase, the integrated sedimentation rate (taking into account compaction) was less than 100 m/My, which translates into heating < 1°C/My for a thermal gradient of 20°C. For this reason, in all inverse models presented the maximal heating/cooling rate has been set to be lower (in most cases) or equal to 3°C/My and the changes in the time-temperature path have been qualified as 'intermediate' in most models.

All models start at 1000 Ma, with the initial temperature between 90°C and 180°C. On a regional scale, this constraint on the pre-Ordovician history of basement samples is supported by geological evidence:

1- The Proterozoic volcanic and sedimentary succession on Belcher Islands in the eastern Hudson Bay were metamorphosed at the prehnite-pumpellyite to subgreenschist facies, indicating that maximum temperatures experienced during the Trans-Hudson orogeny (~1.8 Ga) were in the order of 250-350°C.

2- Study of the reflectance of the organic matter found in Paleoproterozoic sedimentary rocks of the Mistassini Basin (Quebec) indicates that thermal

conditions associated with maximal burial did not exceed 200°C (Héroux et al., 2004).

3- In the Lake Timiskaming area, south of the James Bay, sediments and volcanics of the Paleoproterozoic Huronian Supergroup were metamorphosed at ~1.85-1.9 Ga to sub-greenschist facies conditions.

The goodness of fit for each thermal history was assessed using Kuiper's Statistic. Good fit and acceptable fit paths have goodness-of-fit values of > 0.75 and 0.05, respectively. The best way to consider the paths is that a 'good' fit implies that the time-temperature path is *supported* by the data, while an acceptable time-temperature path is *not ruled out* by the data (Ketcham, 2013). In the following figures, envelopes of good and acceptable fits are shown as overlapping fields (magenta for good fit paths and green for acceptable fit paths) in the time-temperature diagrams. Also shown are peak heating points (magenta for good fit paths and green for acceptable fit paths) within each of the time-temperature constraint boxes. Further, the HeFTy software highlights a "best fit" path (shown as a heavy black line) for modelling runs as well as predicted AFT ages and track length information for that path, which can be readily compared with the measured parameters. Although the best-fit path most closely matches the measured parameters it is emphasized that other time-temperature paths (especially good fit paths) are also possible.

For all inverse models presented in this study, the Monte Carlo modeling ended when 20 good paths had been generated.

5b. Sample 2009-LKA-38 - Narwhal well

A Precambrian gneiss sample from the base of the Narwhal South O-58 well (1310 m depth; < 5 m below the Paleozoic unconformity) yielded a pooled AFT age of 381.2 ± 16.5 Ma (central age 377.1 ± 15.5 Ma). C-axis projected horizontal track lengths range between 10.8 and 15.6 μm and show a unimodal distribution.

Dpar values range from 1.39 to 1.82 μm, with an average of 1.66 μm and a standard deviation of 0.11 μm. No relationship exists between AFT age and Dpar (Fig. 4) suggesting that the annealing kinetics of single grains in the sample are homogeneous. Chlorine content of apatite analysed in 2013 ranges from 0.02 to 0.32% (average 0.14%).
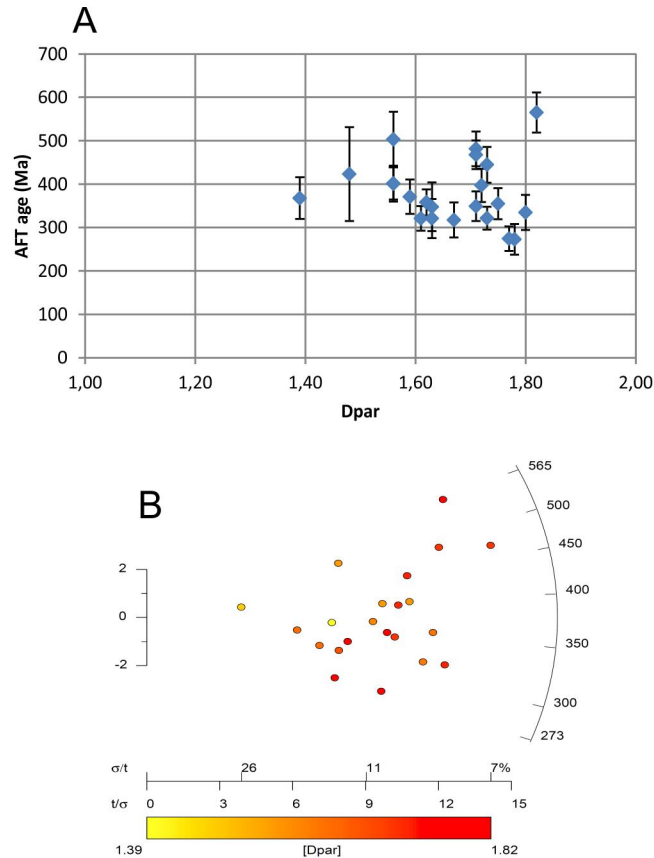
Figure 4: Diagrams showing (A) Dpar versus age and (B) radial plot for the Narwhal well sample. In (B) more precise fission track ages plot further from the origin along the x-axis (precision).

Base model

Thermal history of the base model (Model A) takes into account the following constraints:

- ➢ Sediments found at the base of the well were deposited in shallow water between 457 and 445 Ma (Edenian) in a tropical environment (15-35°C).

- ➢ The topmost part of the preserved succession is Upper Devonian (370-385 Ma). At this time, the base of the succession reached temperatures between ~35 and 75°C. The 35°C limit is based on a decompacted thickness of 1.7 km, geothermal gradient of ~12°C and surface temperature of 15°C. The 75°C limit is based on a geothermal gradient of ~30°C and surface temperature of 25°C. These estimates are considered as end-members.

- ➢ Sediments that postdate the preserved succession (= prolonged low subsidence sedimentation classical on intracratonic basins) are thought to have been deposited between 370 and 300 Ma (based on other North American intracratonic basins). The temperature window of this episode

16

is broadly defined as ~40°-100°C (i.e. with a lower temperature limit only 5°C above the one used for the Upper Devonian).

➢ The present-day temperature at 1.3 km depth is defined as ranging between 18°C and 34°C.

Modeling results suggest that the maximal temperature experienced by the samples was between 66 and 77°C (all good paths; best fit path = 70°C). Taking into account acceptable paths, scenarios with a maximal temperature < 65°C and > 80°C are not permitted by the data. However, the timing of maximum-burial is not well constrained and good fit paths occupy almost all the time interval allowed for late low-subsidence sedimentation.
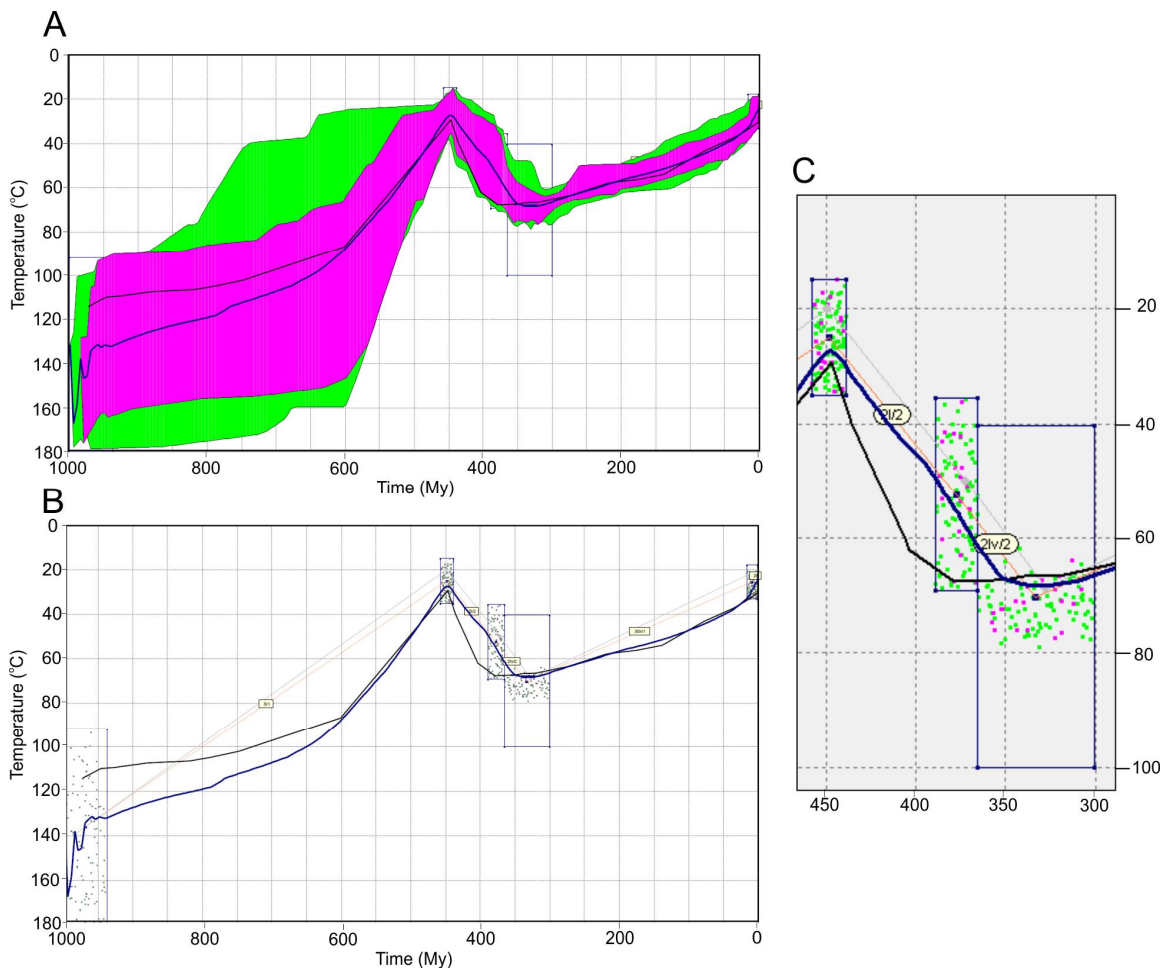
Figure 5: Inverse model results for the base model – Narwhal well. A) Envelopes including all the good paths (magenta) and acceptable paths (green). B) Plot of peak heating points within each of the time-temperature constraint boxes. Good points are magenta, acceptable are green. C) Zoom of B) focussing on the post-Upper Ordovician burial episode. The best fit path is shown as a black line and the weighted mean path as a blue line.

For the best fit path, the reflectance calculated using the Sweeney and Burnham (1990) model is 0.56, in contrast with the vitrinite equivalent reflectance measured at the base of well (~0.70; Bertrand and Malo, 2012). This discrepancy will be discussed in section 6b.

Testing alternative models

The following alternative models have been tested and the results are presented in Figure 6 and Table 3.

- ➢ *Model B-* This model piggybacks on the observation that: a) some good fit paths of model A lie close to the maximum temperature allowed at present, and b) that some good fit paths lie close to the minimum age allowed for the end of sedimentation, suggesting that the model was possibly over constrained. Model B thus allows temperatures up to 38°C at present and sedimentation to continue to 250 Ma instead of 370 Ma (~ Permian-Triassic boundary).
- ➢ *Model C-* This model uses the same time-temperature constraints as the base model, but allows a greater complexity of time-temperature paths. For this model all segments between constraints have 9 nodes, intermediate complexity, and maximum cooling rate of 3°C/Ma.
- ➢ *Model D-* This model could be qualified as the 'maximum constraint' model. Two time-temperature constraints have been add to take into account an upper Silurian-Lower Devonian unconformity (Pinet et al., 2013).
- ➢ *Model E-* This model could be qualified as the 'minimum constraint' model. The time and temperature during the deposition of basal sediments is taken into account as well as maximal burial conditions defined as occurring sometime between 250 and 390 Ma at temperatures between 35 and 100 °C.

Results from these alternative models show that:
- The maximum temperature is relatively well-constrained as all models yielded nearly similar results between ~64 and 81 °C (all good paths) with an average at ~70°C.
- The timing of maximal burial is not well constrained as good fit paths occupy nearly all the time allowed for sedimentation in each model.
- Thermal histories calculated for the model that accounts for an upper Silurian-Lower Devonian period of erosion (unconformity; model D) have post 370 Ma time-temperature paths that are similar to those of other models.
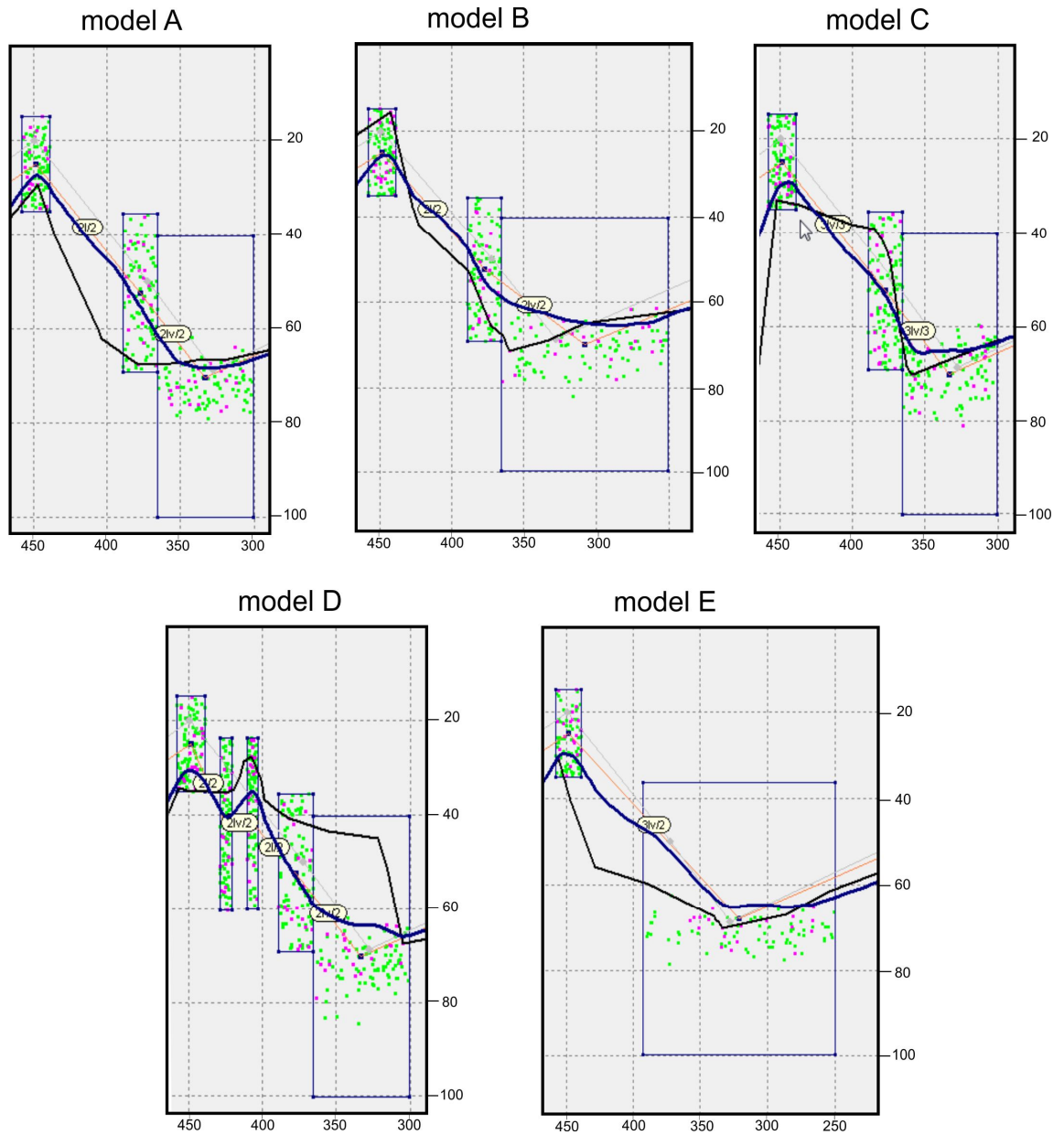
Figure 6: Inverse model results for the base model (A) and alternative models (B to E) – Narwhal well. For each model, a plot of peak heating points within the time-temperature constraint boxes (post-Ordovician burial episode only) is shown. Good points are magenta, acceptable are green. The best-fit path is shown as a black line and the weighted mean path as a blue line.

- The vitrinite reflectance values of the best-fit solutions (highest calculated value among all models of 0.57) are always lower than the measured value (~ 0.70). This discrepancy will be discussed in section 6b.

Model No	aim	Maximal temperature - all good paths (^{o}C)	Maximal temperature - best fit (^{o}C)	time of maximal temperature - all good paths (My)	time of maximal temperature - best fit (My)	GOF age	GOF length	No of runs
2009-LKA-38 (NARWHAL WELL)								
A	base model	66-77 (avg = **71.5**)	70	310-377	377	0.90	0.94	7702
B	larger time-temperature boxes	62-78 (avg = **70**)	70	256-368	359	0.93	0.78	6637
C	greater variability	60-81 (avg = **70.5**)	70	309-375	359	0.96	0.77	8912
D	upper Silurian unconformity	64-79 (avg = **71.5**)	67	306-364	306	0.93	0.84	9204
E	minimal constraints	65-75 (avg = **70**)	71	264-359	333	1.00	0.97	9408
2009-LKA-42 (BELUGA WELL)								
A	base model	62-80 (avg = **71**)	79	258-377	372	0.70	0.72	10507
B	Mesozoic increase in temperature allowed	58-74 (avg = **66**)	67	160-375	160	0.98	0.75	7531
C	upper Silurian unconformity	64-76 (avg = **70**)	65	273-382	315	0.97	0.89	9357
D	minimal constraints	63-74 (avg = **68.5**)	67	175-380	250	0.95	0.88	21359
97-10-395 (MANITOBA)								
A	base model	83-99 (avg = 91)	87	385-437	410	0.92	0.45	500000 - 12 good paths
B	higher temperature allowed in Upper Ordovician	76-96 (avg = 86)	88	345-425	420	0.93	0.57	366803

Model No	aim	Maximal temperature - all good paths (°C)	Maximal temperature best fit (°C)	time of maximal temperature - all good paths (My)	time of maximal temperature - best fit (My)	GOF age	GOF length	No of runs
97-10-393 (MANITOBA)								
A	base model	76-87 (avg = **81.5**)	82	323-437	422	0.96	0.99	137325
B	higher temperature allowed in Upper Ordovician	66-95 (avg **80.5**)	85	315-445	420	0.99	0.89	46793
09SZ-23-01 (MELVILLE PENINSULA)								
A	base model	56-72 (avg = **64**)	62	262-432	264	0.94	0.45	114425
09SZ-21-01L (SOUTHAMPTON ISLAND)								
A	base model	65-85 (avg = **75**)	72	285-420	390	0.95	0.87	18152
B	High temperature in Mesozoic-Cenozoic allowed	65-85 (avg = **75**)	71	255-422	350	0.93	0.94	14666
2009-LKA-15 (AKPATOK)								
A	base model	75-117 (avg = **96**)	85	255-445	413	0.82	0.63	13525
B	High temperature in Mesozoic-Cenozoic allowed	78-112 (avg = **95**)	93	290-452	310	0.95	0.31	7487
C	low Paleozoic maximum heating; High temperature in Mesozoic-Cenozoic allowed	75-80 (avg = **77.5**)	77	308-455	385	0.97	0.56	89790

Table 4: Inverse model results. See text for comments. GOF is a measure of the goodness of fit.

5c- Sample 2009-LKA-42 - Beluga well

A Precambrian gneiss sample has been recovered at the base of the Beluga O-23 well at a depth of 2200 m (< 10 m below the Paleozoic unconformity). This sample yielded a pooled age of 372.1 ± 23.8 Ma (central age 372.2 ± 22.5 Ma). C-axis projected horizontal track lengths range between 10.32 and 14.09 μm and show a unimodal distribution.

Dpar values range from 1.46 to 1.88 μm, with an average of 1.64 μm and a standard deviation of 0.11 μm. No relationship exists between AFT age and Dpar (Fig. 7) suggesting that the annealing kinetics of single grains in the sample is homogeneous.

Chlorine content of apatite grains from the same sample analysed in 2013, ranges from 0.00 to 0.09% (average 0.03%).

Figure 7: Diagrams showing (A) Dpar versus Age and (B) radial plot for the Beluga well sample. In (B) more precise fission track ages plot further from the origin along the x-axis (precision).

Base model

The thermal history of the base model (Model A) takes into account the same constraints as those applied to the Narwhal well, except that the highest possible temperature during the Upper Devonian (topmost part of the preserved succession) is ~80°C. This takes into account the greater thickness of sediments. The present-day temperature at 2.2 km depth is loosely defined as ranging between 30°C and 50°C.

Modeling results suggest that the maximal temperature experienced by the samples is between ~62 and 80°C (all good paths; best fit path = 79°C). Even when acceptable paths are considered, maximal temperatures > 85°C are not permitted by the AFT data.

The timing of burial is not well constrained and some good paths (including the best fit path) reach the maximum temperature in the Upper Devonian (top of the preserved succession) suggesting that the now eroded sedimentatary succession was not so thick.
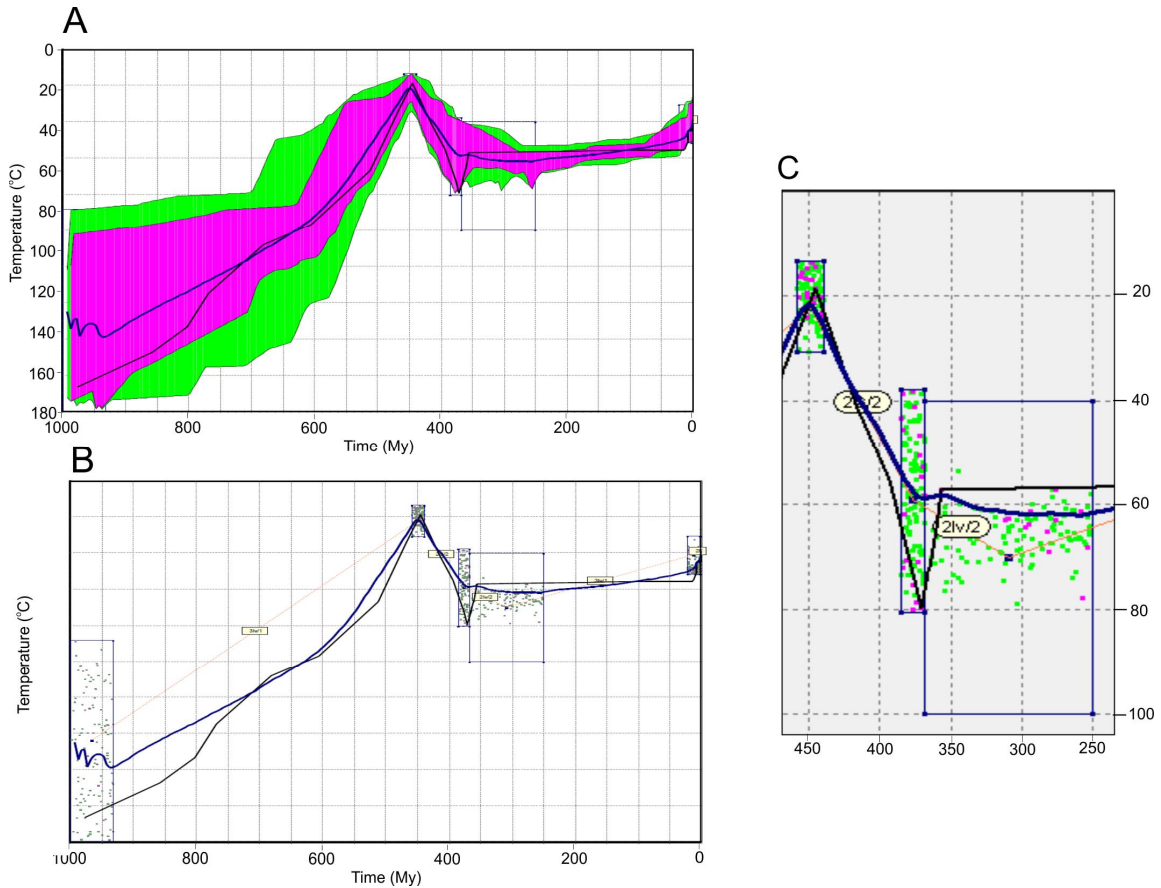
Figure 8: Inverse model results for the base model – Beluga well. A) Envelopes including all the good paths (magenta) and acceptable paths (green). B) Plot of peak heating points within each of the time-temperature constraint boxes. Good points are magenta, acceptable are green. C) Zoom of B) focussing on the post- Upper Ordovician burial episode. The best-fit path is shown as a black line and the weighted mean path as a blue line.

For the best fit path, the organic matter reflectance calculated using the Sweeney and Burnham (1990) model is 0.49, in contrast with the vitrinite equivalent reflectance measured at the base of well (~0.65; Bertrand and Malo, 2012; see section 6b for a discussion).

Testing alternative models
The following alternative models have been tested and the results are presented in Figure 9 and Table 4.

- ➢ *Model B-* This model considers the same time-temperature constraints as the base model, but tests the possibility of an increase in temperature during the Mesozoic (either due to burial or to the passage of the Great Meteor hotspot).
- ➢ *Model C-* Two time-temperature constraints have been added to take into account an upper Silurian-Lower Devonian unconformity (similar to the 'maximum constraint model' for the Narwhal well).
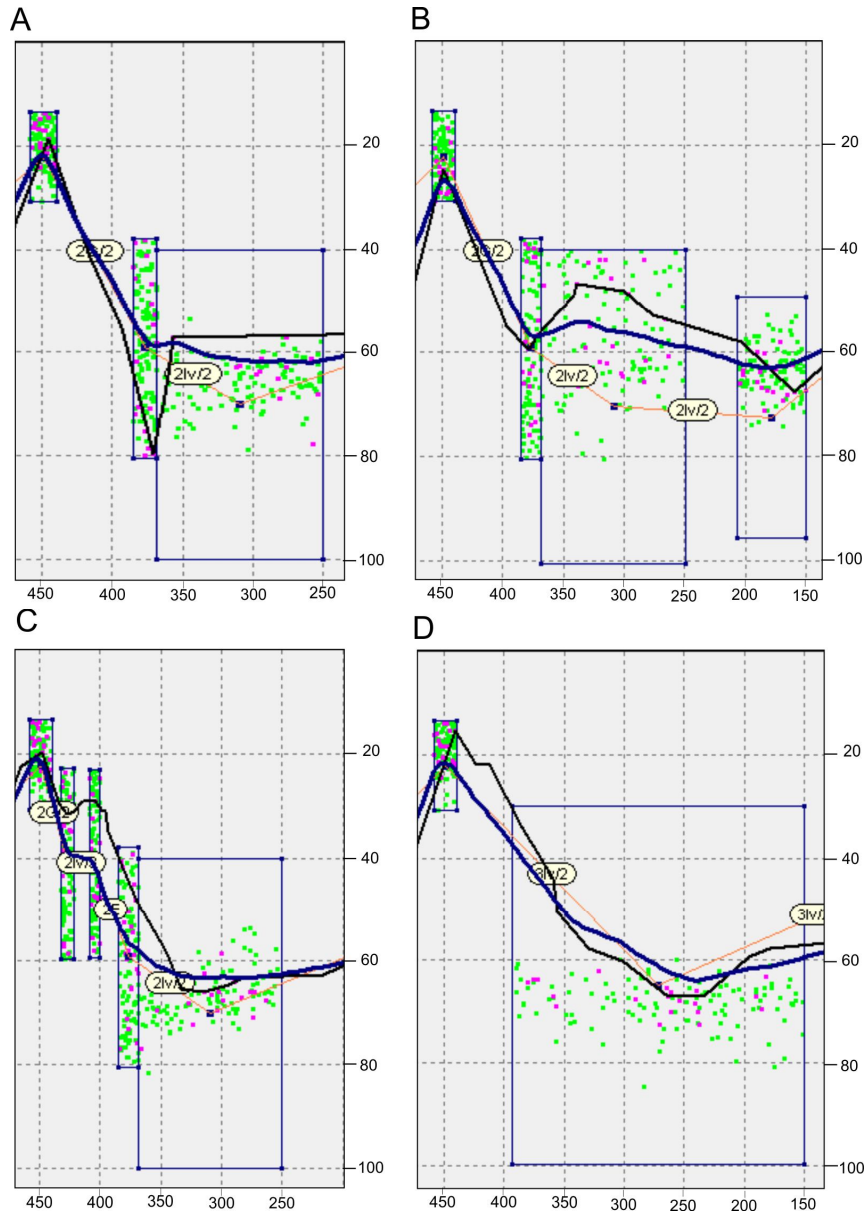
Figure 9: Inverse model results for the base model (A) and alternative models (B to D) – Beluga well. For each model, a plot of peak heating points within the time-temperature constraint boxes (post-Ordovician burial episode only) is shown. Good points are magenta, acceptable are green. The best-fit path is shown as a black line and the weighted mean path as a blue line.

➢ *Model D-* The time and temperature during the deposition of basal sediments is taken into account as well as maximal burial conditions broadly defined as occurring between 200 and 390 Ma and temperatures between 35 and 100°C (similarly to the 'minimum constraint' model for the Narwhal well).

Results from these alternative models show that:
- The 'minimum constraint model' yielded the narrowest range of maximum temperatures (~63-74°C).
- For most models, the envelope of good fit paths shows a very long period (> 200 Ma) with temperature variations of ~10°C or less, consistent with very slow exhumation. For this reason, the timing of maximum temperature is not well defined and could even have occurred during Mesozoic time.
- Highest model maximum temperatures (>73°C) are reached when the peak temperature was reached before 370 Ma. On the other hand, lower maximal temperatures (< 67°C) characterize scenarios with later (<300 Ma) peak temperatures.
- Inverse models may account for an upper Silurian-Lower Devonian period of erosion (unconformity; model C).
- For all models, the vitrinite value of the best-fit solution is lower than the measured vitrinite-equivalent reflectance value.

5d- Sample 97-10-395 (Manitoba)

Sample 97-10-395 is a Precambrian porphyritic granite located in Manitoba, 19 km to the west of the Paleozoic unconformity. This sample yielded a pooled age of 316.5 ± 16.7 Ma (central age 324.8 ± 15.6 Ma). C-axis projected horizontal track lengths range between 11.13 and 15.79 μm. Dpar values range from 1.25 to 1.63 μm, with an average of 1.43 μm and a standard deviation of 0.11 μm. A poorly defined positive correlation exists between AFT age and Dpar (all grains; R^2=0.16; Fig. 10) suggesting that annealing kinetics of single grains may vary slightly. Chlorine content of apatite grains from the same sample (analysed in 2013) is uniformly very low (between 0.00 to 0.03%).

In the base model, the Paleozoic sedimentary cover originally extended over the sample locality with a dip between 0 and 4° (present-day regional dip of ~0.5°), placing the maximum depth of the sample during the Upper Ordovician (*ca.* 450 My) at 1.3 km, which translates to a maximum temperature of ~45°C (for a surface temperature of 25°C and a geothermal gradient of 20°C/km). The post Ordovician time-temperature constraint for this model is limited to 30-100°C between 450 and 300 Ma.
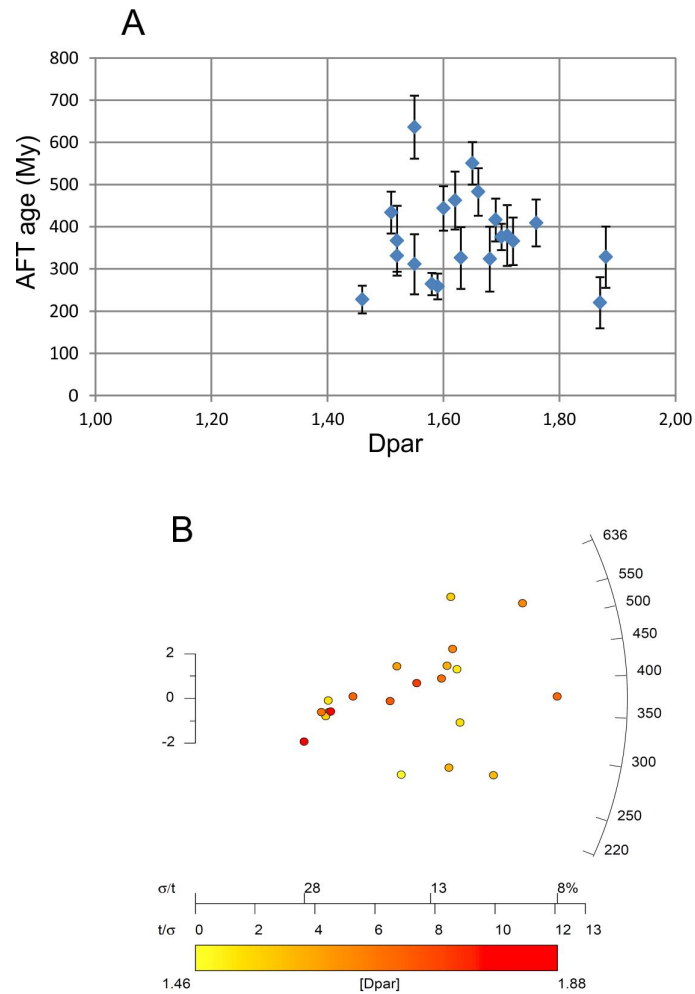
Figure 10: Diagrams showing (A) Dpar versus age and (B) radial plot for the sample 97-10-395 (Manitoba). In (B) more precise fission track ages plot further from the origin along the x-axis (precision).

After 500000 iterations, only 12 good fit paths were generated with geological constraints imposed on the base model. These good fit paths correspond to post-Ordovician maximum temperature between 83 and 99°C (average ~87°C), with only a few acceptable paths with peak temperatures < 80°C (Fig. 11 and Table 3). Interestingly, good and acceptable paths do not cover the entire time range allowed for maximal temperature and post-lowermost Carboniferous (300 Ma) solutions seem excluded.

Alternative model B (Fig. 11 D and E; Table 3), allows for higher temperatures (70°C) during the Ordovician. The twenty good fit paths (generated in 366803 iterations) show striking similarities with the base model and good solutions always exhibit a post-Ordovician peak temperature at ~87 ± 10°C and a restricted interval for maximum temperature. However, the temperature at *ca* 450 Ma is poorly constrained between 28 and 69°C (all good fit paths) and, for this reason, the magnitude of post-Ordovician increase in temperature remains uncertain.
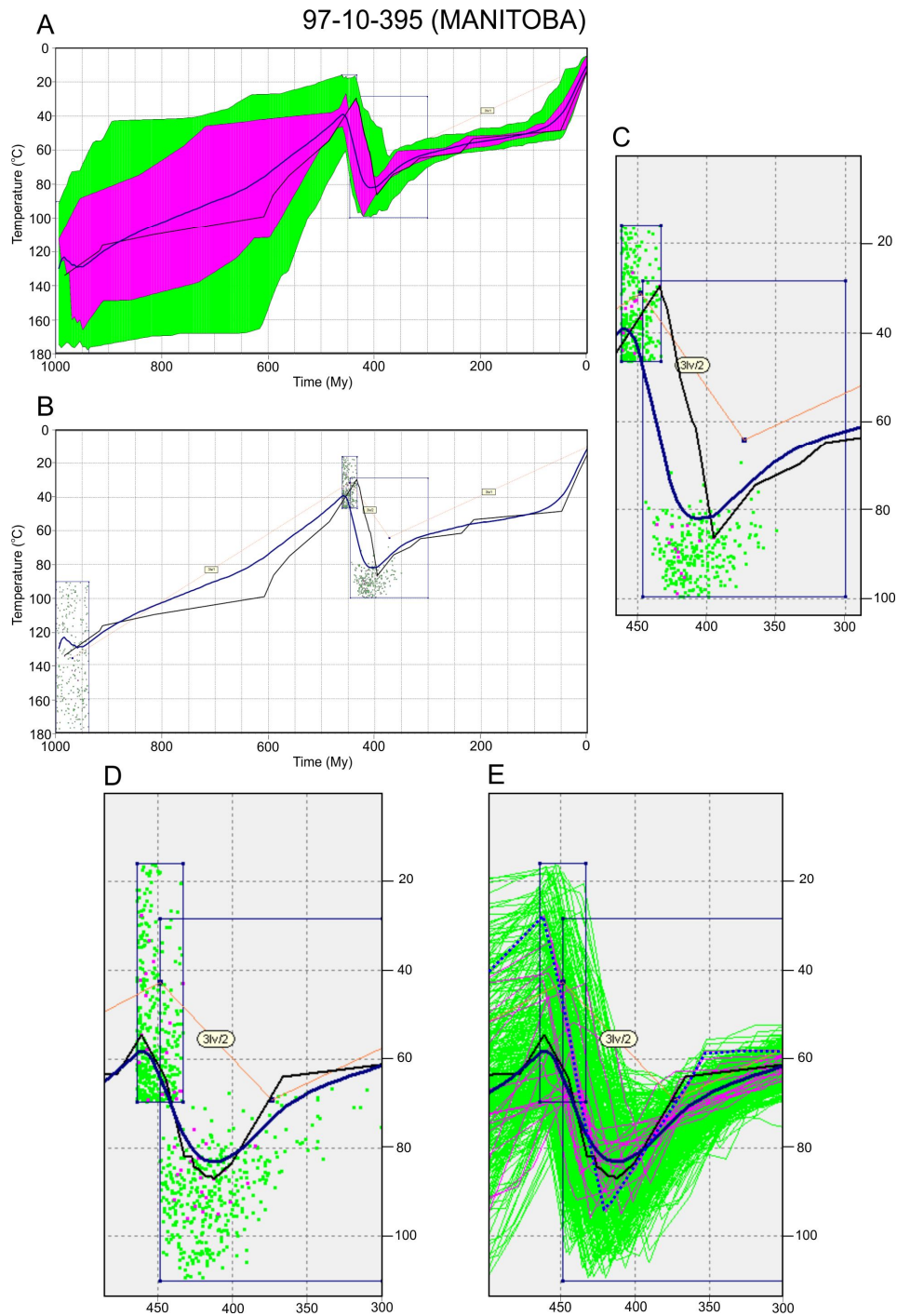
Figure 11: Inverse model results for the base model (A, B and C) and alternative model (D and E) – sample 97-10-395. BASE MODEL: A) Envelopes including all the good paths (magenta) and acceptable paths (green). B) Plot of peak heating points within each of the time-temperature constraint boxes. C) Zoom of B) focussing on the post- Upper Ordovician burial episode. ALTERNATIVE MODEL: D) Plot of peak heating points; D) Plot of good and acceptable paths. Good points are magenta, acceptable are green. The best-fit path is shown as a black line and the weighted mean path as a blue line.

5e- Sample 97-10-393 (Manitoba)

Sample 97-10-393 is a Precambrian porphyritic granite located in Manitoba, 32 km to the west of the Paleozoic unconformity (~ 14 km away from sample 97-10-395). This sample yielded a pooled age of 359.0 ± 12.1 Ma (central age 358.6 ± 11.4 Ma). C-axis projected horizontal track lengths range from 10.45 and 15.85 μm.

Dpar values range from 1.17 to 1.50 μm, with an average of 1.37 μm and a standard deviation of 0.08 μm. A poorly defined positive correlation exists between AFT age and Dpar (all grains; R^2=0.09; Fig. 12) suggesting that annealing kinetics of single grains may vary slightly. Chlorine content of apatite grains from the same sample (analysed in 2013) ranges from 0.00 to 0.07% (average 0.02%).

The base model (Fig. 13 and Table 4) uses the same time-temperature constraints as the base model for sample 97-10-395 (corresponding in this case to a maximum regional dip of the Paleozoic cover of *ca.* 2°). Results indicate that post-Ordovician maximum temperature was ~76-87°C (all good fits). Several good fit paths lie close to the base of the Upper Ordovician time-temperature box suggesting that the model may be over constrained.

Figure 12: Diagrams showing (A) Dpar versus Age and (B) radial plot for the sample 97-10-393 (Manitoba). In (B) more precise fission track ages plot further from the origin along the x-axis (precision).

Figure 13: Inverse model results for the base model (A to C) and alternative model B (D) – Sample 97-10-393. A) Envelopes including all the good paths (magenta) and acceptable paths (green).B) Plot of peak heating points within each of the time-temperature constraint boxes. Good points are magenta, acceptable are green. C) Zoom of B) focussing on the post- Upper Ordovician burial episode. The best-fit path is shown as a black line and the weighted mean path as a blue line. D) Plot of peak heating points for alternative model B.

Alternative model B (Fig. 14 and Table 3) tests this possibility by allowing Upper Ordovician (~450 Ma) maximum temperature up to 70°C. In this model, good fit paths exhibit post 440 Ma peak temperatures between ~66 and 95°C and (in contrast with sample 97-10-395) cover almost all the allowed time interval. The temperature at *ca*

450 Ma is poorly constrained between 22 and 67°C (all good fit paths) and for this reason the magnitude of post-Ordovician temperature increase remains uncertain.

5e- Sample 09SZ-23-01 (Melville Peninsula)

Sample 09SZ-23-01 is a Precambrian gneiss located in the Melville Peninsula close (< 200 m) to the contact with the Paleozoic unconformity. This sample yielded the oldest age among the studied sample with a pooled age of 462.7 ± 29.9 Ma (central age 485.5 ± 26.7 Ma). It also yielded the oldest single grain age (731.5 ± 88.8 Ma). C-axis projected horizontal track lengths range from 11.33 to 15.05 μm.

Dpar values range from 1.41 to 2.06 μm, with an average of 1.67 μm (the highest value among the seven samples studied) and a standard deviation of 0.16 μm. AFT age and Dpar show no correlation (Fig. 14). Chlorine content of apatite grains from the same sample (analysed in 2013) ranges from 0.02 to 0.12% (average 0.05%).
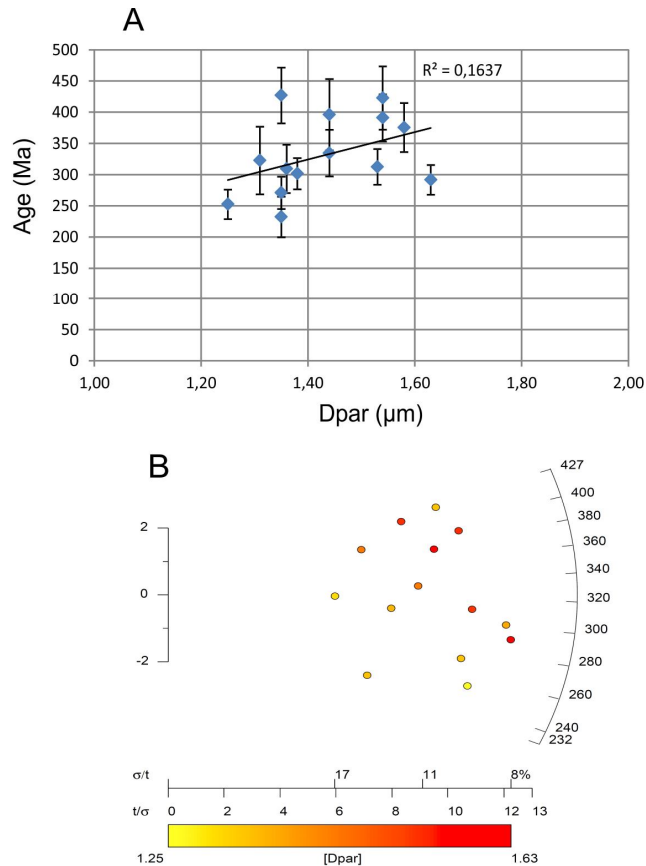

Figure 14: Diagrams showing (A) Dpar versus Age and (B) radial plot for sample 09SZ-23-01 (Melville Peninsula). In (B) more precise fission track ages plot further from the origin along the x-axis (precision).

Thermal history of the base model (Fig. 15 and Table 4) takes into account the fact that nearby Paleozoic sediments were deposited at shallow water depth in a tropical environment (15-35°C), during the Middle Ordovician (*ca.* 465 Ma). Heating following initial deposition is very broadly defined both in time (250-465 Ma) and temperature (~22-100°C). Considering the lack of additional geologically-based constraints, no alternative models were tested.
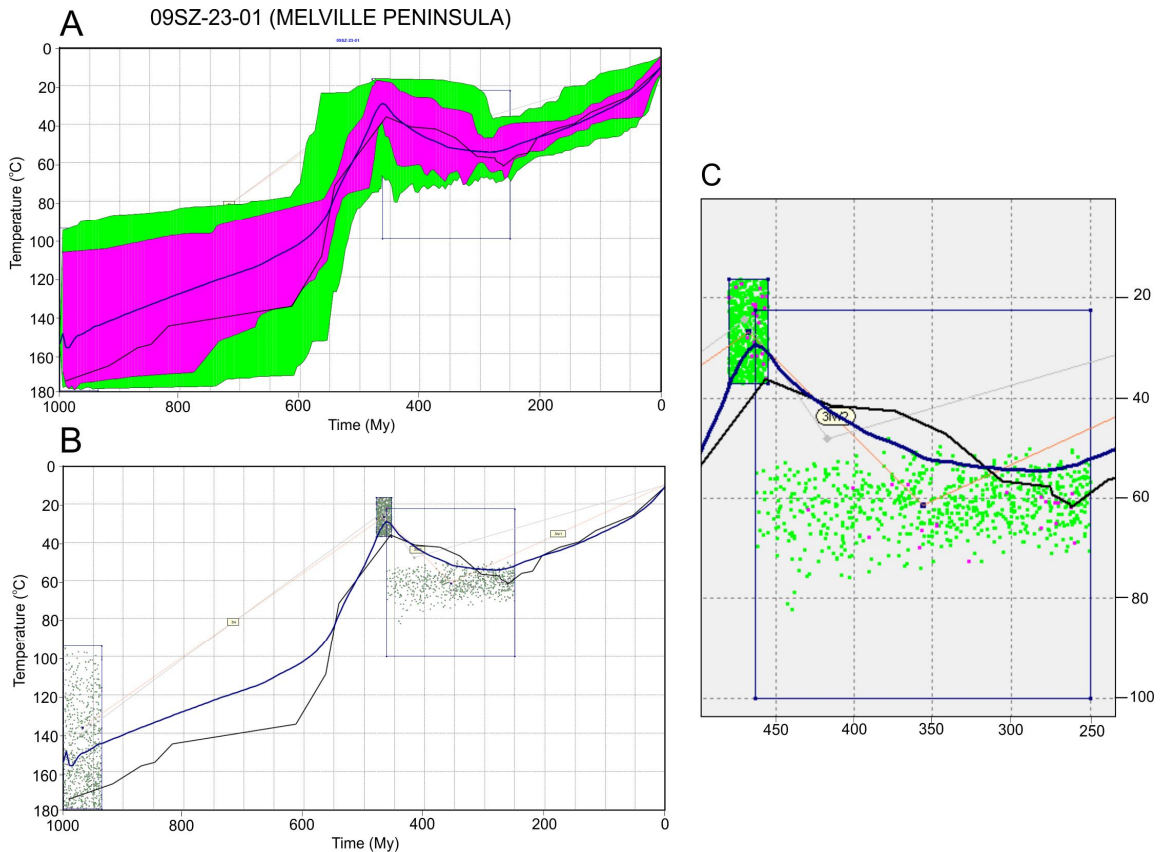
Figure 15: Inverse model results for sample 09SZ-23-01 (Melville Peninsula). A) Envelopes including all the good paths (magenta) and acceptable paths (green).B) Plot of peak heating points within each of the time-temperature constraint boxes. Good points are magenta, acceptable are green. C) Zoom of B) focussing on the post- Upper Ordovician burial episode. The best-fit path is shown as a black line and the weighted mean path as a blue line.

The inverse model indicates that maximal temperature was 64° ± 8°C and that temperatures > 78°C are not permitted by the AFT data (even considering acceptable fit paths). The timing of maximum heating is not well constrained.

5f – Sample 09SZ-21-01L – Southampton Island

Sample 09SZ-21-01L is an Ordovician sandstone located at the base of the sedimentary succession on Southampton Island (Fig. 1). Only 15 grains were suitable for AFT analysis. This sample yielded a pooled age of 395.2 ± 24.5 Ma (central age 393.0 ± 23.0 Ma). C-axis projected horizontal track lengths range from 10.66 to 16.00 µm.

Dpar values range from 1.21 to 1.83 µm, with an average of 1.56 µm and a standard deviation of 0.18 µm. The diagram Dpar vs AFT age shows no correlation (Fig. 16) indicating that the annealing kinetics of single grains in the sample is rather similar. Chlorine content of apatite grains analysed in 2013 ranges from 0.02 to 0.30% (average 0.13%).
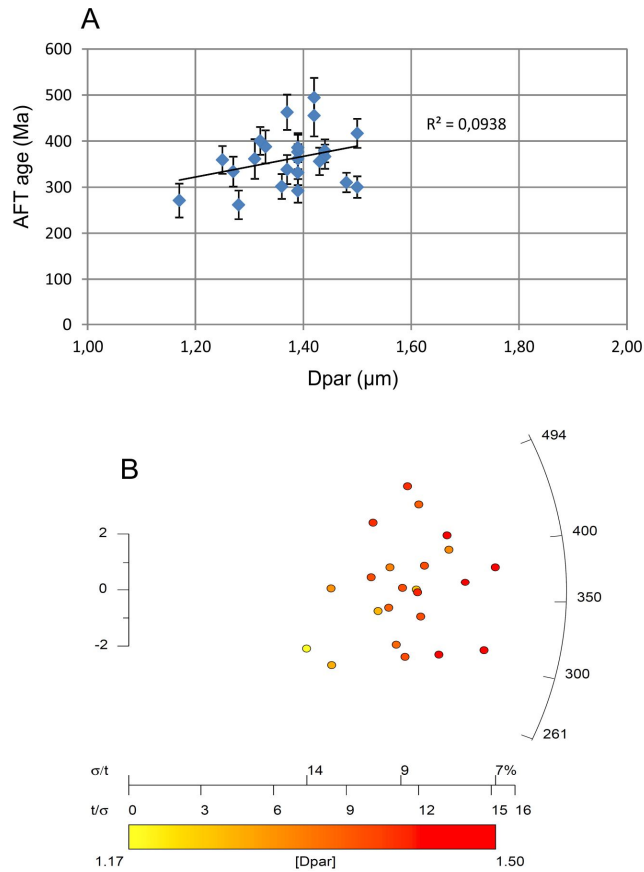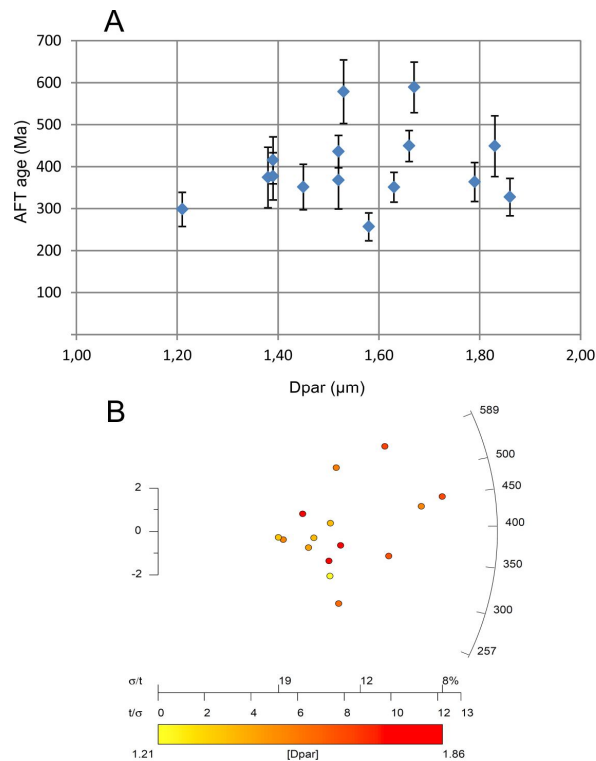

Figure 16: Diagrams showing (A) Dpar versus Age and (B) radial plot for sample 09SZ-21-01L (Southampton Island). In (B) more precise fission track ages plot further from the origin along the x-axis (precision).

The thermal history of the base model (Model A) takes into account the sandstone deposition at shallow water depths in a tropical environment (15-35°C) and a burial episode that is very broadly defined both in time (250-450 Ma) and temperature (10-100 °C). Results indicate that post-Ordovician maximum temperature was ~65-85°C (all good fits), with the best fit at ~72°C. Maximum heating occurred during the late Silurian – Early Permian (all good fits), with the best fit falling at ~390 My (Middle Devonian, Fig. 17 and Table 4).
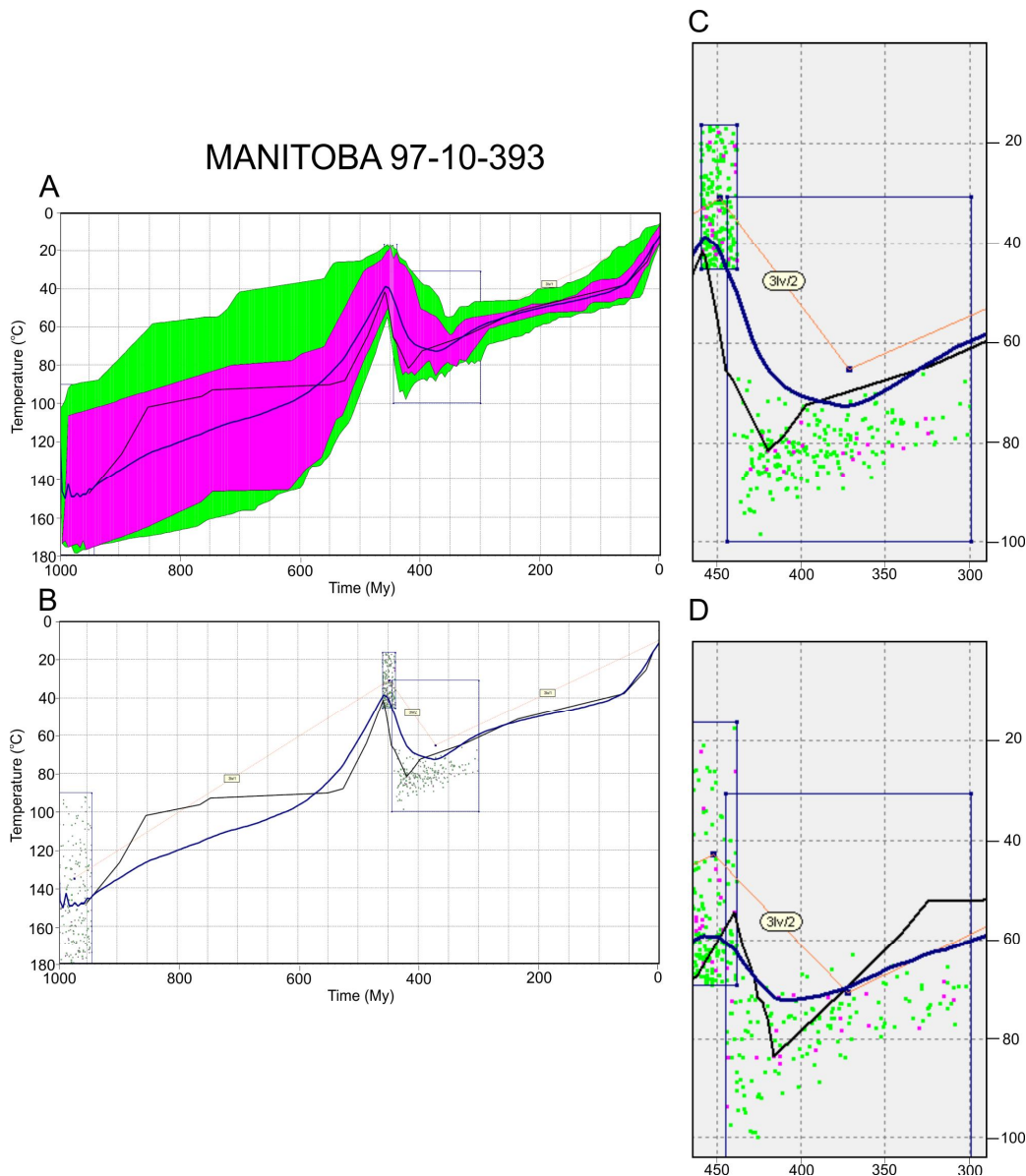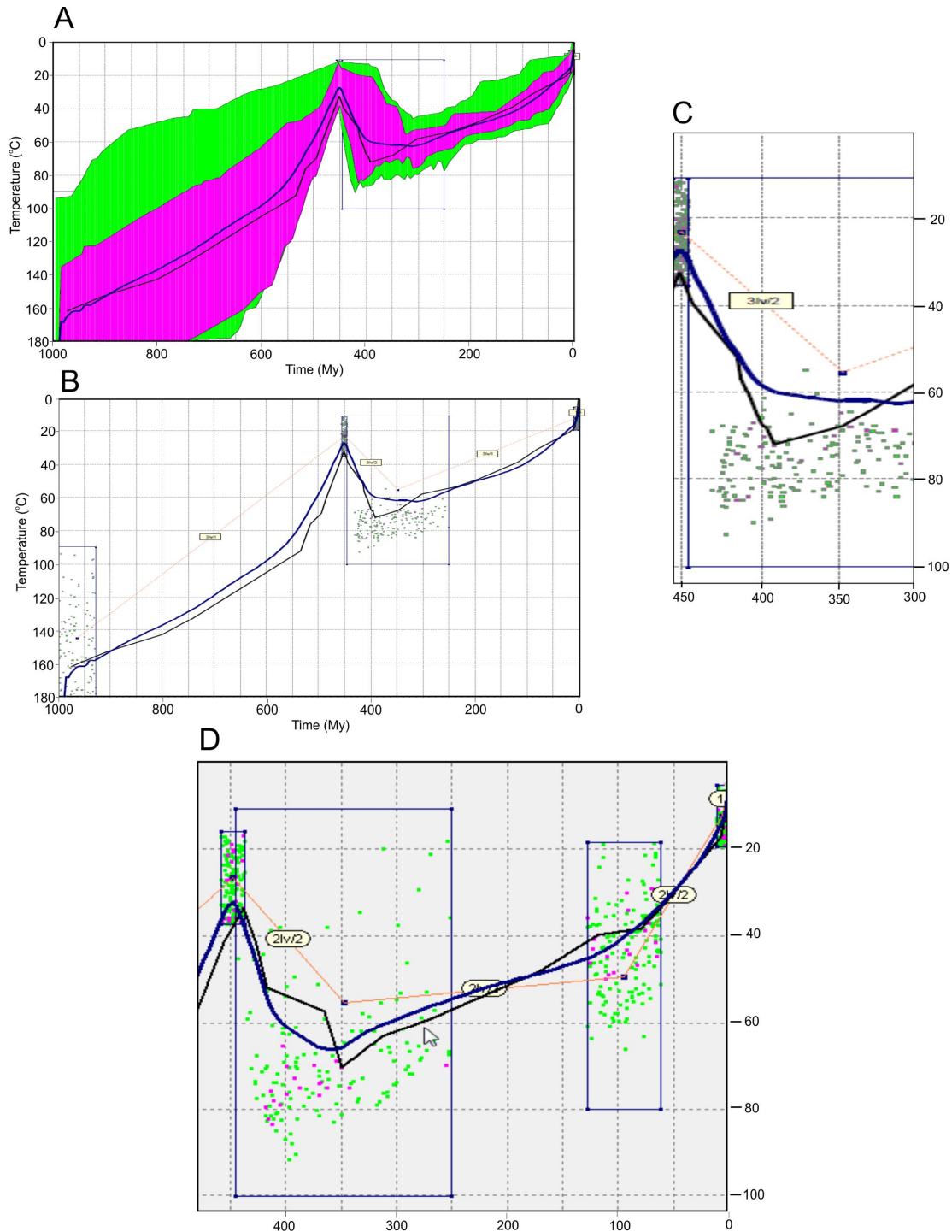
Figure 17: Inverse model results for the base model (A to C) and alternative model B (D) – sample 09SZ21-01L. A) Envelopes including all the good paths (magenta) and acceptable paths (green). B) Plot of peak heating points within each of the time-temperature constraint boxes. Good points are magenta, acceptable are green. C) Zoom of B) focussing on the post-Upper Ordovician burial episode. The best-fit path is shown as a black line and the weighted mean path as a blue line. D) Plot of peak heating points for alternative model B.

Alternative model B tests the possibility of an episode of relatively high temperature during the Mesozoic. Results are almost identical to those for Model A and no good fits show temperatures >50°C at 100 Ma (Fig. 18 and Table 3).

The vitrinite reflectance of the best fit using the Sweeney and Burnham (1990) organic model maturation model is 0.58 relatively close to the values reported in Lavoie et al. (2013) for the shale intervals at Cape Donovan (maximal value = 0.56).

5g- Sample 2009-LKA-15– Akpatok well

Sample 2009-LKA-15 is a Precambrian gneiss located at the base of the Akpatok L-26 well at a depth of 340 m (< 5 from the Paleozoic unconformity). This sample yielded a pooled age of 215.1 ± 15. Ma (central age 230.6 ± 13.5 Ma), the youngest among samples studied.

Dpar values range from 1.15 to 1.86 µm, with an average of 1.42 µm and a standard deviation of 0.16 µm. Plots for Dpar vs AFT age (Fig. 18) show no correlation (or even a poorly defined negative correlation; R^2 = 0.12) indicating that annealing kinetics of single grains in the sample are rather homogeneous. Chlorine content of apatite grains from the same sample (analysed in 2013) is uniformly low (< 0.04%)

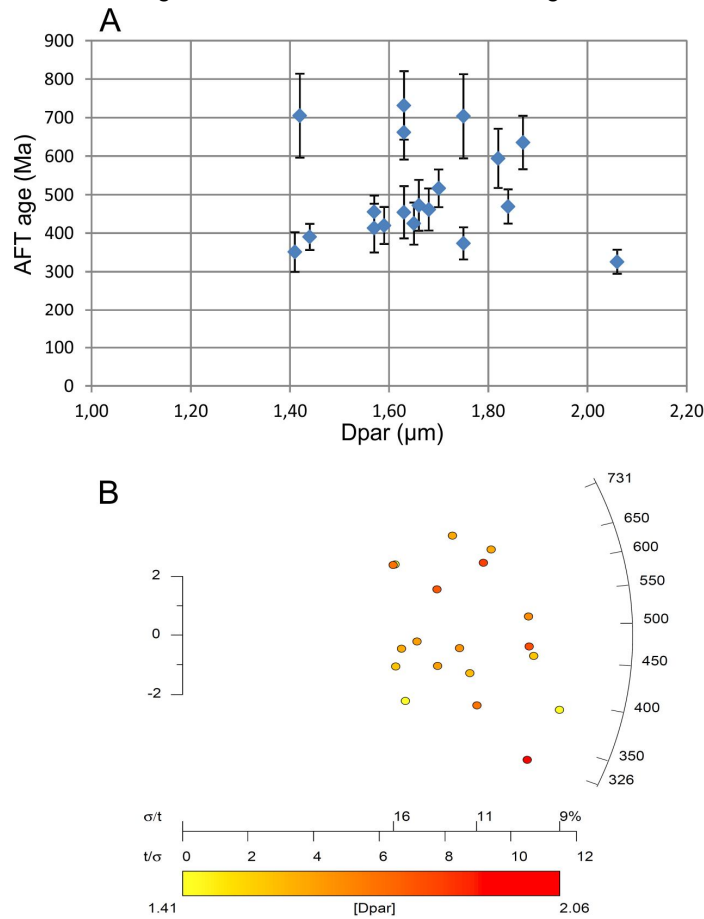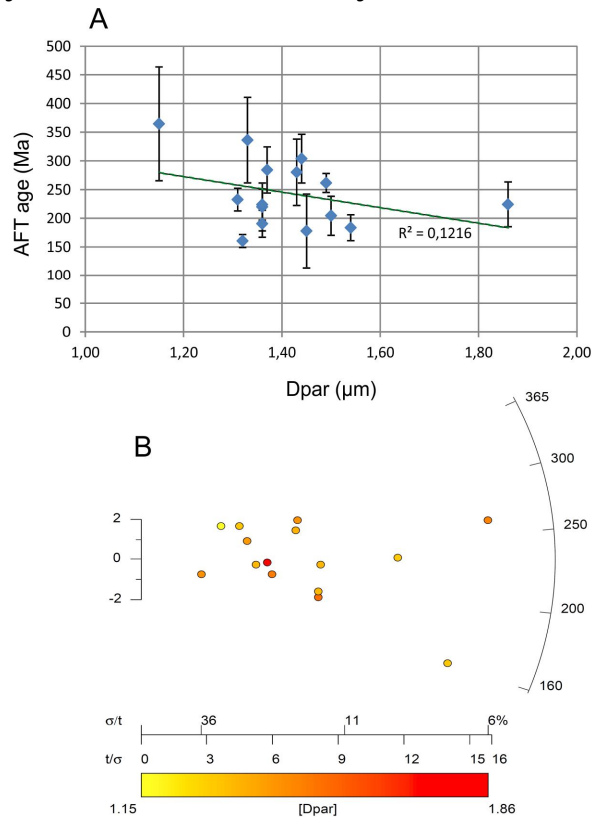*Figure 18: Diagrams showing (A) Dpar versus age and (B) radial plot for sample 2009-LKA-15. In (B) more precise fission track ages plot further from the origin along the x-axis (precision).*

The thermal history of the base model (Model A) takes into account the late Early Ordovician age (ca. 475 My) of basal sediments that were deposited in shallow water depths in a tropical environment (15-35°C) and considers very broadly defined maximal heating conditions sometime between 460 and 250 Ma, with temperatures between 15 and 120 °C.

The maximum temperatures of the base model thermal solutions are more variable than those of other samples with the maximum temperatures reached by good fit paths spread over a ~40°C temperature interval (77-117°C) (Fig. 19 and Table 4). The higher temperature part of the good fit path envelope is the highest among the seven samples studied. Timing of maximum heating is not well defined and good fit paths occupy almost the entire time interval permitted.
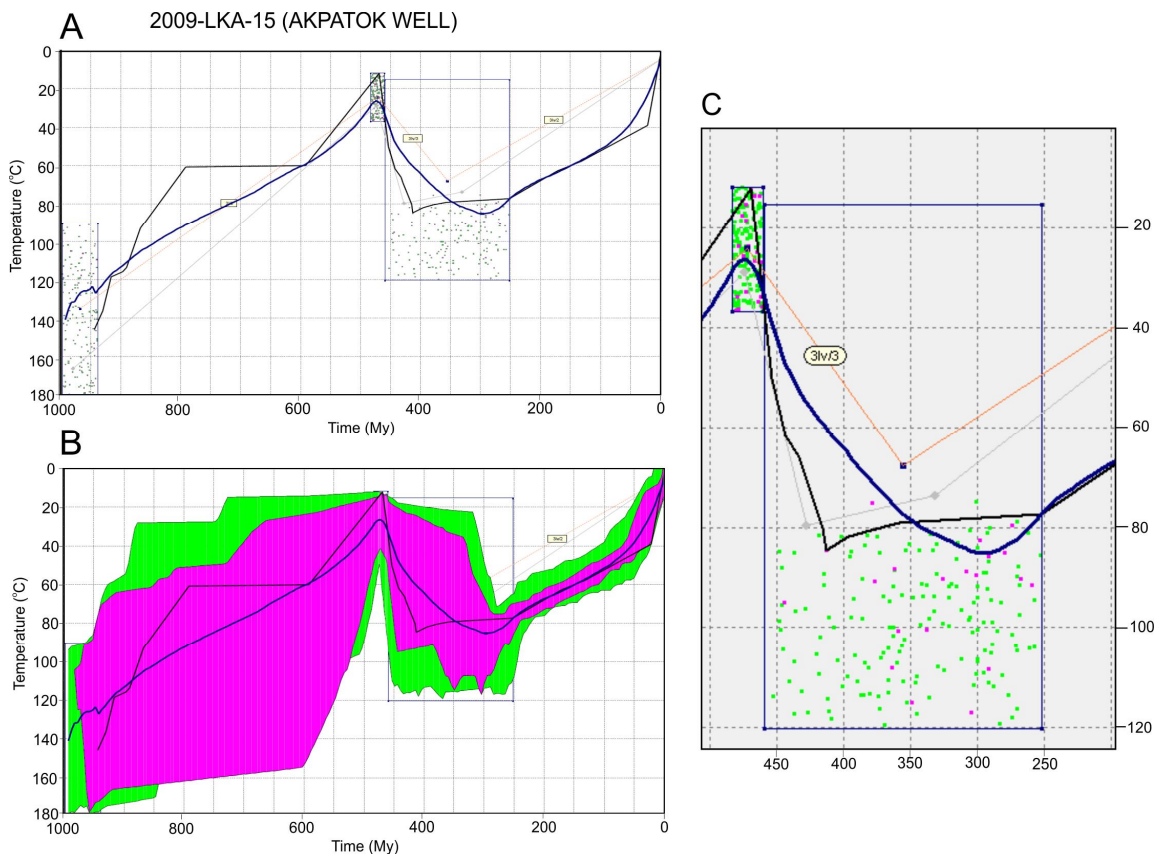
Figure 19: Inverse model results for the base model for Akpatok well. A) Envelopes including all the good paths (magenta) and acceptable paths (green). B) Plot of peak heating points within each of the time-temperature constraint boxes. Good points are magenta, acceptable are green. C) Zoom of B) focussing on the post- Upper Ordovician burial episode. The best-fit path is shown as a black line and the weighted mean path as a blue line.

Alternative model B tests the possibility of an episode of reheating during the Mesozoic-early Cenozoic, possibly linked with the opening of the Labrador Sea (Fig. 20 and Table 3). Results are almost identical to those for Model A and temperatures greater than 65°C at 100 Ma seem excluded.
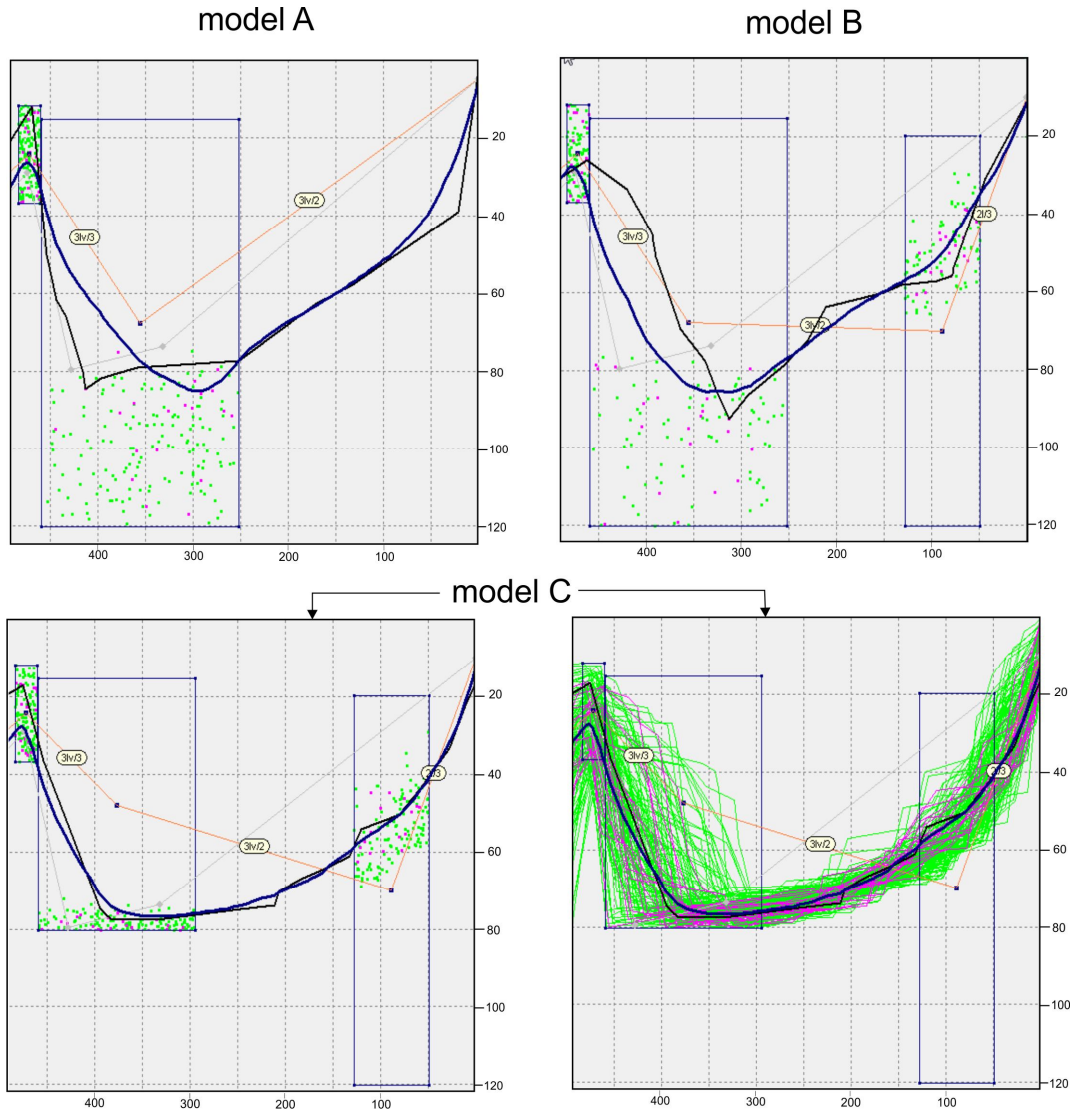
Figure 20: Inverse model results for the base model (A) and alternative models (B and C) – Akpatok well. For each model, a plot of peak heating points within the time-temperature constraint boxes (post-Ordovician history only) is shown. Good points are magenta, acceptable are green. The best-fit path is shown as a black line and the weighted mean path as a blue line. Note the almost identical shape of all acceptable and good fit paths for model C (bottom right).

Alternative model C imposes relatively low temperatures (<80°C) during the Paleozoic and allows higher temperatures during the Mesozoic-early Cenozoic (Fig. 20

and Table 4). Results indicate that all good fit paths that satisfy the constraints have a near identical shape, with ca. 200 My of residence in the 75-80°C temperature interval.

6- Discussion

6a- Modelling strategies

During inverse modelling, special attention has been paid to not over constrain the models.

For the samples from the Narwhal, Beluga and Akpatok wells, and the samples collected close to the Paleozoic unconformity (Melville Peninsula and Southampton Island), the time-temperature box corresponding to the deposition of the base of the succession is a very robust constraint. The Ordovician constraint is probably less certain in the case of the base models for the Manitoba samples, but based on geological considerations we consider it reasonable.

Additional constraints have been added to the Narwhal and Beluga base models, based on the sedimentary record at these localities. These constraints are reasonable and not too strictly defined. An indirect indication of this statement is provided *a contrario* by minimum constraint models that show very similar results.

Moreover, rapid changes in temperature (> 3°C/My) have been precluded as they would be difficult to justify in intra-continental setting.

In most cases, possible variations in the annealing kinetics of analyzed apatite grains do not seem to be an issue. Average chlorine content is relatively uniform and low, ranging from 0.01 to 0.14%, and indicates that the analysed grains are fluorapatite. For these reasons, any justification for dividing the apatite grains into several populations would be questionable.

6b- Comparison with organic matter maturation data

Vitrinite reflectance data is an ideal complement to AFT analysis, as it provides an independent way to estimate maximum temperatures. For typical apatite, total annealing of fission tracks typically corresponds to vitrinite reflectance values of ~ 0.7% over heating times of ~ 10 My (Green and Duddy, 2012). Vitrinite being absent in pre-Devonian rocks, organic maturation is determined using dispersed organic matter and then translated to a vitrinite-*equivalent* value (Bertrand and Malo, 2012).

In the case of the Narwhal and Beluga wells, vitrinite reflectance calculated using the time-temperature path inferred from AFT modeling and the equations developed by Sweeney and Burnham (1990) are lower (for the base and alternative models) than the measured vitrinite *equivalent* values (Bertrand and Malo, 2012) near the base of the sedimentary succession.

If observations (reflectance; track analysis) and measurements (U concentration) are correct, this discrepancy may result from several factors:

- An inaccurate conversion of reflectance measurements done on dispersed organic matter (organoclasts) to a vitrinite equivalent value; such inaccuracy could be related to imprecise organoclast-vitrinite reflectance conversion equation or the thermal effect of rock matrix (clastic vs carbonate) on organoclast reflectance;

- An inadequacy of the organic matter maturation model of Sweeney and Burnham (1990) in the case of very long (>200 Ma) period of residence at moderate temperatures (50-70°C);

- Changes in annealing or diffusion behavior (or both) of apatite in the case of long-term low-temperature thermal history. This hypothesis, first proposed by Hansen and Reiners (2006), remains controversial in the AFT community.

- Heating of the base of the sedimentary succession by relatively hot basinal fluids (resulting in relatively high vitrinite *equivalent* values) that did not interact with the impermeable Precambrian basement (resulting in relatively low maximum temperatures in AFT inverse models).

The discrepancy between the calculated vitrinite reflectance and the measured vitrinite *equivalent* reflectance should encourage a cautious approach, especially for interpretations that associate reflectance values/temperatures with petroleum generation stages.

In the case of the Akpatok well, Tmax values on Rock Eval analysis average 431°C and classify the base of the well as 'immature'. Most of the AFT inverse modeling good fit paths and especially those with maximum temperature > 90°C are irreconcilable with such a state of maturation.

6c- Role of thermal gradient and burial in reaching maximum heating conditions

Two main regional factors may contribute to reach maximum heating conditions: an increase of the geothermal gradient and/or an increase in depth due to burial. The conversion from a thermal frame of reference (AFT data) to an absolute frame of reference (depth) would require constraining paleo-temperatures at surface and paleo-thermal gradients. In the Hudson Bay region, data needed for such conversion are lacking and only a qualitative discussion may be considered.

The Hudson Bay region is presently characterized by very low thermal gradients. However, higher gradients likely prevailed during crustal thinning and mantle ascent in the Upper Ordovician (?) to late Early Devonian period. Geothermal gradients probably decreased exponentially when extension ceased and relaxed to relatively low values in

50 My or less, as predicted by numerical models (Mareschal, 1987).

In view of the aforegoing, two-end member scenarios may account for AFT inverse modeling results for the Narwhal well (Fig. 22).
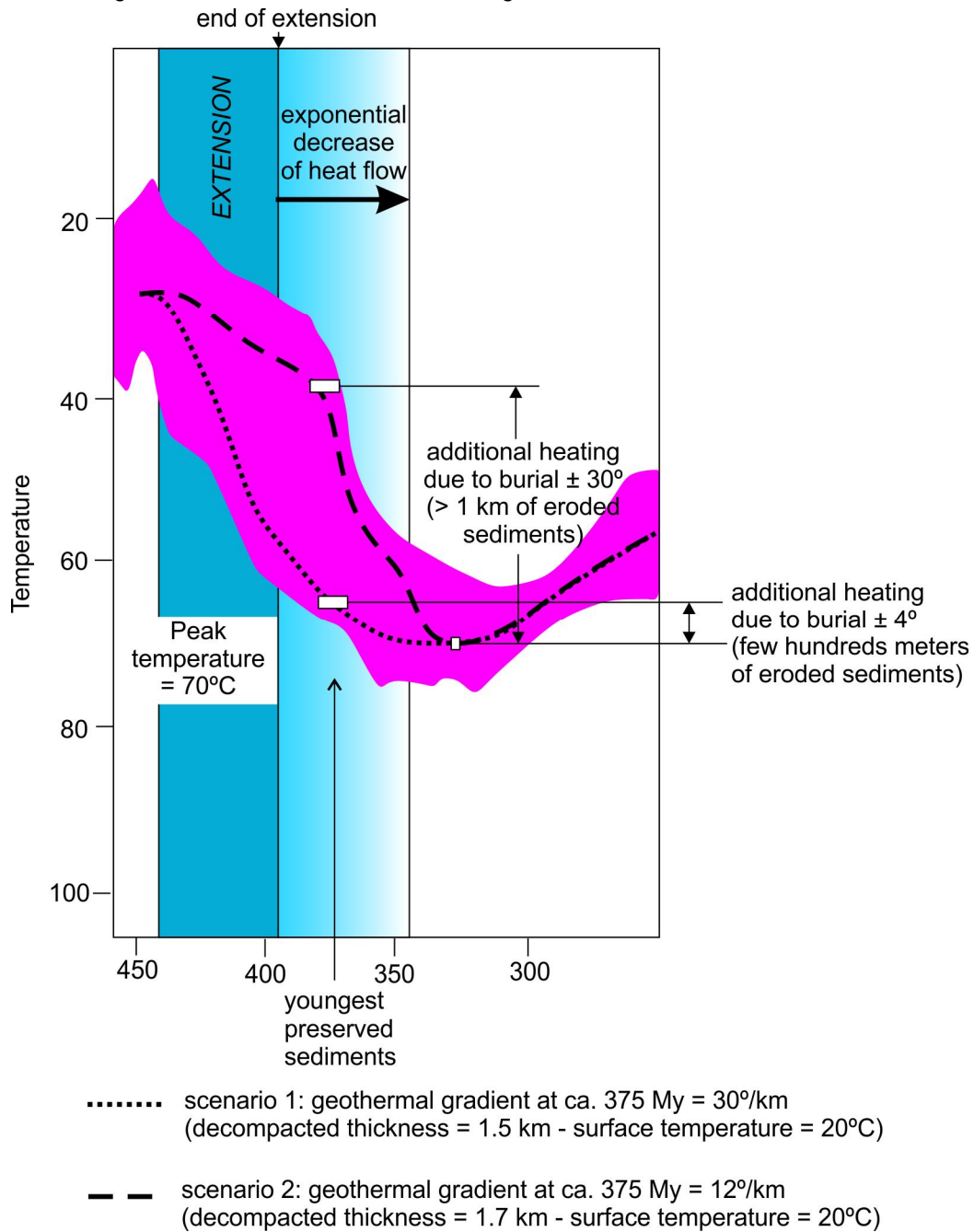
Figure 21: Time-temperature scenarios used for the Narwhal well to discuss the thickness of sediment younger than the preserved succession that may have been eroded. See text for comment. The magenta envelope includes all the good fit paths for the base model.

In the first scenario, the Late Devonian geothermal gradient, some 25 My after cessation of extension, was still high (around 30°/km for a decompacted thickness of 1.5 km and a surface temperature of 20°C). In this scenario, at ca. 375 My (top of the preserved succession), the temperature attained ~66°C, only ~4°C higher than the average maximum temperature calculated from fission track data, suggesting that additional burial by sediments now eroded was minimal (a few hundred meters).

In the second scenario, the geothermal gradient in Late Devonian relaxed to very low values that characterize the present-day thermal state of some parts of the craton (around 12°/km for a decompacted thickness of 1.7 km and a surface temperature of 20°C). In this scenario, the temperature reached at *ca.* 375 My (top of the preserved succession), was ~40°C, some 30°C lower than the average maximum temperature, suggesting that additional burial by sediments now eroded was significant (>> 1 km).

As already mentioned, these scenarios are end-members and the geothermal gradient in Late Ordovician was probably between 30°C/km and 12°C/km.

In the case of the Beluga well, the presence of a thick (ca. 900 m) salt unit brings an additional complexity as it would probably disturb the isotherms, with temperature values lower than regional average below the salt. Numerical modeling by Zhao and Lerche (1993) indicates that salt sheets may have significant impacts on temperature in underlying formations, with a predicted lowering of temperature by 10.5°C underneath a 1000 m thick salt interval (as calculated for specific values of heat flow and conductivities used in Zhao and Lerche, 1993).

A recent low-temperature geochronology study (AFT and (U-Th)/He analysis; Taylor and Fitzgerald, 2011) suggests that the passage of the Adirondack region over the Great Meteor Hotspot led to the establishment of an elevated geothermal gradient, possibly followed by thermal doming, increase in erosion rate and relaxation of isotherms. This host spot was located on the western side of the present-day Hudson Bay between 220 and 170 Ma, and some inverse models investigated the possibility of significant heating during this period. Our results however indicate that the thermal effects of the passage of the Great Meteor hotspot, if any, were limited or not developed on a regional scale.

7- Summary and Perspective

The low-temperature (60-120°C) thermal history of seven samples from the Hudson Bay region has been investigated using apatite fission track (AFT) analysis. Six samples are from Precambrian rocks sampled either at surface or at the bottom of hydrocarbon-targeted wells and one sample is from a thin sandstone unit lying at the base of the Paleozoic succession. All AFT ages are younger than the age of their host

rock indicating that samples experienced significant post-crystallisation or deposition annealing and were subjected to temperatures > 60°C. The track length distributions suggest slow cooling.

With the exception of the Akpatok well sample, all samples have AFT ages and mean horizontal confined track lengths that are broadly in agreement with those previously documented in the southern Canadian Shield (see the Plate 1 of Kohn et al., 2005).

Inverse modeling results suggest that during the Paleozoic the samples from Southampton Island and eastern Manitoba experienced similar or even higher temperatures than samples from the central part of the basin (Narwhal and Beluga wells). This is somewhat surprising and underscores our poor understanding of the late history of the basin. However, we should keep in mind that AFT results are not the first to hold a few surprises, as the highest recorded organic matter maturation values (Reyes et al., 2011; in press) are found in northern Ontario (INCO-Winisk well), some 500 km south of the (present-day) center of the basin.

Clearly, more data are needed to clarify the thermal history of the Canadian Shield, to decipher regional trends and constrain the timing of maximum heating. These issues are critical for the hydrocarbon assessment of the area.

8. Acknowledgment

9. References

Bertrand, R., Malo, M., 2012. Dispersed organic matter reflectance and thermal maturation in four hydrocarbon exploration wells in the Hudson Bay Basin: regional implication. Geological Survey of Canada, Open File 7066, 54 p.

Carlson, W.D. Donelick, R.A. and Ketcham, R.A. 1999. Variability of apatite fission-track annealing kinetics: I. Experimental results. American Mineralogist, 84, 1213-1223.

Cookenboo, H.O., Orchard, M.J., Doaud, D.K., 1998. Remnants of Paleozoic cover on the Archean Canadian Shield: limestone xenoliths from kimberlite in the central Slave craton. Geology, 26, 391-394.

Donelick, R.A., O'Sullivan, P.B., Ketcham, R.A., 2005. Apatite fission track analysis. Reviews in Mineralogy and Geochemistry, 58, 49-94.

Eaton, D.W., Darbyshire, F., 2009. Lithospheric architecture and tectonic evolution of the Hudson Bay region, Tectonophysics, 480, 1-22.

Ehlers, T.A., Chaudhri, T., Kumar, S., Fuller, C.W., Willet, S., Ketcham, R.A., Brandon, M.T., Belton, D.X., Kohn, B.P., Gleadow, A.J.W., Dunai, T.J., Fu, F.Q., 2005.

Computational tools for low-temperature thermochronometer interpretation. Review in Mineralogy & Geochemistry, 58, 589-622.

Galbraith, R.F. 2005. *Statistics for fission track analysis*. Chapman & Hall/CRC, Boca Raton, USA, 219 p.

Galbraith, R.F. and Laslett, G.M. 1993. Statistical models for mixed fission track ages. Nuclear Tracks, 21, 459-470.

Gallagher, K., 2012. Transdimensional inverse thermal history modeling for quantitative thermochronology. Journal of Geophysical Research, 117, B02408.

Gallagher, K., Brown, R., Johnson, C., 1998. Fission track analysis and its applications to geological problems. Annual Review Earth and Planetary Sciences, 26, 519-572.

Gleadow, A.J.W., Belton, D.X., Kohn, B.P., Brown, R.W., 2002. Fission track dating of phosphate minerals and the thermochronology of apatite. *In* Kohn, M., Rakovan, J. and Hugues, J.M. (eds.) Phosphates – Geochemical, Geobiological and Material importance, Reviews in Mineralogy and Geochemistry, 48, 579-630.

Gleadow, A.J.W. Gleadow, S.J. Belton, D.X. Kohn, B.P. Krochmal, M.S. 2009. Coincidence Mapping - a key strategy for automated counting in fission track dating. *In* Lisker, F., Ventura, B. and Glasmacher, U.A. (*eds*). *Thermochronological Methods: From Palaeotemperature Constraints to Landscape Evolution Models.* Geological Society, London, Special Publications 324, 25–36.

Gleadow, A,J.W., Harrison, M., Kohn, B., Lugo-Zazueta, R., Phillips, D., 2015. The Fish Canyon Tuff: a new look at an old low-temperature thermochronology standard. Earth and Planetary Science Letters, 424, 95-108.

Green, P.F., Duddy, I.R., 2012. Thermal history reconstruction in sedimentary basins using apatite fission-track analysis and related techniques. *In*: Analysing the thermal history of sedimentary basins: method and case studies, SEPM Special Publication No 103, p. 65-104.

Hansen, K., Reiners, P.W., 2006. Low temperature thermochronology of the southern East Greenland continental margin: evidence from apatite (U-Th)/He and fission track analysis and implication for intermethod calibration. Lithos, 92, 117-136.

Hasebe, N. Barberand, J. Jarvis, K. Carter, A. and Hurford, A. 2004. Apatite fission-track thermochronometry using laser ablation ICP-MS. Chemical Geology, 207, 135-145.

Héroux, Y., Diagana, B., Chagnon, A., R-Laflèche, M., Moar, R, Houle, P., 2004. Potentiel minéral du Bassin de Mistassini : une réevaluation basée sur des outils empruntés de l'exploration pétrolière. Rapport Divex, 15 p.

Issler, D.R., 1996. An inverse model for extracting thermal histories from apatite fission-track data: instruction and software for Window 95 environment. Geological Survey of Canada, Open File 2325, 84 p.

Ketcham, R.A., 2005. Forward and inverse modeling of low-temperature thermochronometry data. Review in Mineralogy and Geochemistry, 58, 275-314.

Ketcham, R.A. Carter, A. Donelick, R.A. Barbarand, J. and Hurford, A.J. 2007. Improved modeling of fission-track annealing in apatite. American Mineralogist, 92, 799–810.

Ketcham, R.A., 2013. HeFTy, version 1.8.2. Manual user dated 2 october 2013.

Kohn, B.P., Gleadow, A.J.W., Brown, R.W., Gallagher, K., Lorencak, M., Noble, W.P., 2005. Visualizing thermotectonic and denudation histories using apatite fission track thermochronology. Reviews in Mineralogy and Geochemistry, 58, 527-565.

Lavoie, D., Pinet, N., Dietrich, J., Zhang, S., Hu, K., Asselin, E., Chen, Z., Bertrand, R., Galloway, J., Decker, V., Budkewitsch, P., Amstrong, D., Nicolas, M., Reyes, J., Kohn, B.P., Duchesne, M.J., Brake, V., Keating, P., Craven, J., Roberts, B., 2013. Geological framework, basin evolution, hydrocarbon system data and conceptual hydrocarbon plays for the Hudson Bay and Foxe basins, Canadian Arctic. Geological Survey of Canada, Open File 7363, 200 p.

Lavoie, D., Pinet, N., Dietrich, J., Chen, Z., 2015. The Paleozoic Hudson Bay Basin in northern Canada: new insights into hydrocarbon potential of a frontier intracratonic basin: American Association of Petroleum Geologist Bulletin, 99, 859-888.

Mareschal, J.-C., 1987. Subsidence and heat flow in intracontinental basins and passive margins. *In*: Beaumont, C., and Tankard, A.J. (Eds): Sedimentary basins and basin-forming mechanisms, Canadian Society of Petroleum Geologists, Memoir 12, 519-527.

McCracken, A.D., Amstromg, D.K., Bolton, T.E., 2000. Conodonts and corals in kimberlite xenoliths confirm a Devonian seaway in central Ontario and Quebec. Canadian Journal Earth Sciences, 37, 1651-1663.

Osadetz, K.G., Kohn, B.P., Feinstein, S., and O'Sullican, P.B., 2002. Thermal history of Canadian Williston basin from apatite fission-track thermochronology – implications for petroleum systems and geodynamic history. Tectonophysics, 349, 221-249.

Pinet, N., Lavoie, D., Dietrich, J., Hu, K., Keating, P., 2013. Architecture and subsidence history of the Hudson Bay intracratonic basin. Earth-Science Review, 125, 1-23.

Pinet, N. 2016. Far-field effects of Appalachian orogenesis: A view from the craton. Geology, 44, 83-86.

Reyes, J., Armstrong, D., Lavoie, D. 2011. Organic petrology of James Bay Basin. Ontario Petroleum Institute, 50th Annual meeting.

Reyes, J., Jiang, C., Lavoie, D., Milovic, M., Robinson, R., Zhang, S., Armstrong, D., and Mort, A. in press. Determination of Hydrocarbon Generation and Expulsion Temperature of Organic-rich Upper Ordovician Shale from Hudson Bay and Foxe basins using Modified Hydrous Pyrolysis, Organic Petrography and Rock-Eval . Geological Survey of Canada, Open File

Snowdon, L. R., 1995, Rock-Eval Tmax suppression: Documentation and amelioration: American Association of Petroleum Geologists Bulletin, 79, 1337-1348.

Sweeney, J. and Burnham, A.K. 1990. Evaluation of a simple model of vitrinite reflectance based on chemical kinetics. American Association of Petroleum Geologists Bulletin, 74, 1559-1570.

Taylor, J.P., Fitzgerald, P.G., 2011. Low-temperature thermal history and landscape development of the eastern Adirondack Mountains, New York: constraints from apatite fission-track thermochronology and apatite (U/Th)He dating. Geological Society of America Bulletin, 123, 412-426.

Vermeesch, P., Tian, Y., 2014. Thermal history modelling: HeFTy vs. QTQt. Earth Science Reviews, 139, 279-290.

Willet, S.D., 1997. Inverse modeling of annealing of fission tracks in apatite1: a controlled random search method. American Journal of Science, 297, 939-969.

Zhao, K., Lerche, I., 1993. Salt insertions in sedimentary sequences: impacts on temperature and thermal maturation with depth. Terra Nova, 5, 174-185.

Zhang, S., Pell, J., 2014. Conodonts recovered from the carbonate xenoliths in the kimberlites confirm the Paleozoic cover on the Hall Peninsula, Nunavut. Canadian Journal Earth Sciences, 51, 142-155.

ANNEX: AFT RESULTS

Note: microprobe data for apatite grains studied in 2013 are available on request.

Sample: **LKA-38**

Rock Type:						Mineral:		Apatite
Longitude/Latitude:						Elevation (m):		
Calibration X/Y (µm/px):		0.0873/0.0873				^{238}U Standard:		NIST612
Date analysed:		06-mai-2016				Software:		FastTracks v2.17.19

No.	Ns	Area (cm^2)	ρs (cm^{-2})	^{238}U (ppm)	±	1σ	Dpar	Age (Ma)	±	1σ
1	218	3,641E-05	5,988E+06	20,29	±	0,94	1.82 ±0.21	565,1	±	46,4
2	74	1,930E-05	3,835E+06	14,67	±	0,75	1.56 ±0.20	503,0	±	63,9
3	123	4,206E-05	2,924E+06	14,14	±	0,71	1.56 ±0.35	401,1	±	41,4
4	215	5,255E-05	4,092E+06	16,39	±	0,78	1.71 ±0.17	481,2	±	40,0
5	130	3,555E-05	3,657E+06	20,42	±	0,89	1.71 ±0.17	348,8	±	34,2
6	17	3,760E-05	4,521E+05	2,07	±	0,17	1.48 ±0.38	422,9	±	108,3
7	67	5,175E-05	1,295E+06	9,30	±	0,39	1.78 ±0.31	272,8	±	35,2
8	106	2,921E-05	3,629E+06	19,03	±	0,87	1.59 ±0.27	370,8	±	39,8
9	43	1,688E-05	2,547E+06	14,28	±	0,76	1.63 ±0.30	347,4	±	56,1
10	79	3,355E-05	2,355E+06	13,71	±	0,61	1.80 ±0.22	334,9	±	40,5
11	268	4,821E-05	5,559E+06	22,95	±	0,82	1.71 ±0.34	467,4	±	33,1
12	211	3,398E-05	6,210E+06	27,00	±	1,70	1.73 ±0.26	444,6	±	41,5
13	248	7,722E-05	3,211E+06	19,50	±	1,00	1.73 ±0.26	321,4	±	26,2
14	189	6,798E-05	2,780E+06	16,91	±	0,84	1.61 ±0.29	320,9	±	28,3
15	66	3,389E-05	1,947E+06	10,30	±	0,47	1.39 ±0.25	367,6	±	48,3
16	171	4,301E-05	3,976E+06	21,63	±	0,80	1.62 ±0.33	357,7	±	30,4
17	82	2,818E-05	2,910E+06	17,90	±	1,10	1.67 ±0.29	317,4	±	40,1
18	116	3,956E-05	2,932E+06	20,93	±	0,96	1.77 ±0.34	274,4	±	28,4
19	117	3,511E-05	3,333E+06	18,29	±	0,75	1.75 ±0.34	354,7	±	35,9
20	131	2,039E-05	6,426E+06	31,40	±	1,30	1.72 ±0.39	397,1	±	38,4
21	59	2,114E-05	2,790E+06	16,98	±	0,91	1.63 ±0.20	320,7	±	45,2
22	147	2,700E-05	5,445E+06	26,30	±	1,10	1.56 ±0.21	401,5	±	37,1
	2877	8,305E-04	3,559E+06	17,93	±	6.33[a]	1.66 ± 0.11[a]			

[a] Standard deviation of mean

χ^2 = 20.37 (21 degrees of freedom)

P(χ^2) = 49.82 %

Dispersion = 16 %

Pooled Age	**=**	**381,2**	**±**	**16.5 Ma**
Central Age	**=**	**377,1**	**±**	**15.5 Ma**

TRACK LENGTH DATA - LKA-38

No.	Track length (microns)	Angle to c-axis
1	12,11	75,59
2	11,04	46,10
3	11,88	58,19
4	11,36	60,59
5	5,81	61,21
6	12,11	50,58
7	11,23	32,04
8	9,27	44,92
9	11,69	72,64
10	13,31	69,42
11	12,91	49,85
12	15,00	70,62
13	6,77	57,10
14	13,71	61,90
15	12,00	19,44
16	13,43	47,87
17	8,79	79,81
18	9,26	62,73
19	10,25	77,65
20	10,76	12,66
21	13,62	75,35
22	6,65	53,78
23	9,48	70,30
24	13,29	69,33
25	7,83	45,27
26	12,68	66,83
27	11,06	55,55
28	8,39	61,40
29	11,95	49,53
30	11,49	85,14
31	11,84	71,78
32	10,79	48,59
33	12,27	85,30
34	14,08	80,58
35	10,62	64,00
36	9,13	68,48

37	8,26	61,48
38	13,17	74,86
39	5,60	58,97
40	10,53	79,92
41	13,28	34,46
42	11,00	42,22
43	11,67	71,35
44	13,33	55,23
45	10,74	61,56
46	10,25	61,98
47	11,54	72,96
48	10,72	53,95
49	12,12	56,40
50	11,90	51,69
51	10,46	80,53
52	12,12	75,18
53	12,97	44,19
54	13,02	53,42
55	12,02	67,15
56	13,46	76,92
57	11,97	70,85
58	5,08	71,00
59	14,34	75,26
60	10,02	63,88
61	10,55	69,87
62	10,10	32,61
63	9,78	48,98
64	11,49	81,47

Sample: **LKA-42**

Rock Type:				Mineral:	Apatite
Longitude/Latitude:				Elevation (m):	
Calibration X/Y (μm/px):		0.0873/0.0873		^{238}U Standard:	NIST612
Date analysed:		07-mai-2016		Software:	FastTracks v2.17.19

No.	N_S	Area (cm^2)	ρ_S (cm^{-2})	^{238}U (ppm)	±	1σ	Dpar	Age (Ma)	±	1σ
1	61	6,581E-05	9,270E+05	8,02	±	0,55	1.46 ±0.26	227,3	±	33,0
2	85	3,458E-05	2,458E+06	10,97	±	0,40	1.51 ±0.30	433,5	±	49,6
3	80	4,862E-05	1,645E+06	7,17	±	0,29	1.60 ±0.23	443,5	±	52,7
4	21	2,551E-05	8,233E+05	4,93	±	0,25	1.63 ±0.27	325,8	±	73,0
5	20	3,323E-05	6,018E+05	3,78	±	0,19	1.55 ±0.10	311,0	±	71,3
6	81	7,242E-05	1,119E+06	5,21	±	0,26	1.69 ±0.41	416,1	±	50,7
7	14	3,280E-05	4,268E+05	3,82	±	0,25	1.87 ±0.76	219,8	±	60,5
8	89	3,642E-05	2,444E+06	14,42	±	0,57	1.52 ±0.32	330,6	±	37,4
9	83	2,499E-05	3,321E+06	25,20	±	1,10	1.59 ±0.20	258,5	±	30,5
10	158	7,145E-05	2,211E+06	7,70	±	0,35	1.65 ±0.20	550,4	±	50,4
11	88	5,706E-05	1,542E+06	6,16	±	0,29	1.66 ±0.31	482,4	±	56,2
12	67	5,992E-05	1,118E+06	5,30	±	0,31	1.76 ±0.23	408,9	±	55,4
13	51	2,508E-05	2,034E+06	8,50	±	0,42	1.62 ±0.22	461,9	±	68,6
14	19	2,484E-05	7,650E+05	4,62	±	0,28	1.68 ±0.34	323,1	±	76,7
15	50	3,104E-05	1,611E+06	8,57	±	0,52	1.72 ±0.20	365,6	±	56,3
16	119	5,256E-05	2,264E+06	16,81	±	0,69	1.58 ±0.24	264,0	±	26,5
17	31	5,176E-05	5,989E+05	3,07	±	0,19	1.71 ±0.38	379,0	±	72,0
18	208	1,039E-04	2,002E+06	10,36	±	0,47	1.70 ±0.22	375,6	±	31,1
19	21	2,486E-05	8,449E+05	4,48	±	0,25	1.52 ±0.21	366,8	±	82,6
20	22	2,814E-05	7,819E+05	4,65	±	0,27	1.88 ±0.51	328,0	±	72,5
21	86	3,986E-05	2,157E+06	6,46	±	0,30	1.55 ±0.22	635,8	±	74,6
	1454	9,449E-04	1,509E+06	8,10	±	5.27[a]	1.64 ±0.11[a]			

[a] Standard deviation of mean

χ^2 = 18.91 (20 degrees of freedom)
P(χ^2) = 52.79 %
Dispersion = 23 %

Pooled Age	**=**	**372,1**	**±** **23.8 Ma**
Central Age	**=**	**372,2**	**±** **22.5 Ma**

TRACK LENGTH DATA - LKA-42

No.	Track length (microns)	Angle to c-axis
1	8,86	61,25
2	11,58	50,17
3	11,20	65,57
4	11,45	47,95
5	13,24	48,77
6	11,25	66,80
7	11,66	80,26
8	12,07	81,45
9	9,40	80,95
10	11,27	58,10
11	11,95	69,93
12	11,29	73,04
13	13,20	39,63
14	9,29	62,40
15	12,00	41,61
16	10,38	41,78
17	9,35	80,25
18	12,45	67,16
19	11,92	38,64
20	10,41	47,64
21	6,60	63,92
22	9,45	24,84
23	7,90	63,33
24	7,29	64,63
25	10,89	53,76
26	11,34	78,65
27	12,44	69,50
28	11,38	75,65
29	10,19	62,34
30	11,22	50,60
31	7,98	49,39
32	11,60	73,12
33	10,15	54,77
34	10,82	64,03
35	9,56	79,41
36	8,10	77,88
37	10,67	78,57
38	7,66	54,64

39	4,96	51,25
40	7,81	53,11
41	9,60	81,68
42	14,88	81,13
43	7,49	88,38
44	9,35	62,49
45	11,88	46,75
46	11,66	74,72
47	9,99	89,46
48	10,88	83,88
49	11,40	65,25
50	11,38	82,90
51	8,43	71,69
52	11,06	74,67
53	9,43	64,92
54	10,25	68,73
55	12,30	75,58
56	10,85	52,19
57	9,67	53,90
58	10,65	81,22
59	8,94	78,29
60	9,88	78,32

Sample: 393

Rock Type:						Mineral:		Apatite
Longitude/Latitude:						Elevation (m):		
Calibration X/Y (µm/px):		0.0873/0.0873				^{238}U Standard:		NIST612
Date analysed:		19-avr-2016				Software:		FastTracks v2.17.16

No.	N_S	Area (cm^2)	ρs (cm^{-2})	^{238}U (ppm)	±	1σ	Dpar	Age (Ma)	±	1σ
1	223	5,614E-05	3,972E+06	16,58	±	0,82	1.37 ±0.20	462,4	±	38,5
2	168	4,615E-05	3,641E+06	24,40	±	1,00	1.39 ±0.22	291,9	±	25,5
3	190	4,035E-05	4,709E+06	27,70	±	1,10	1.39 ±0.22	331,5	±	27,4
4	127	4,238E-05	2,997E+06	15,48	±	0,70	1.39 ±0.17	376,2	±	37,5
5	341	7,357E-05	4,635E+06	29,20	±	1,20	1.48 ±0.25	310,1	±	21,1
6	187	4,654E-05	4,018E+06	21,78	±	0,90	1.25 ±0.16	359,0	±	30,2
7	112	3,127E-05	3,582E+06	19,30	±	1,40	1.31 ±0.24	361,1	±	43,0
8	151	4,409E-05	3,425E+06	19,74	±	0,88	1.37 ±0.16	338,2	±	31,4
9	169	3,924E-05	4,307E+06	23,20	±	1,00	1.39 ±0.21	361,2	±	31,8
10	270	8,171E-05	3,304E+06	17,55	±	0,67	1.44 ±0.19	366,2	±	26,3
11	338	9,771E-05	3,459E+06	17,74	±	0,66	1.44 ±0.19	378,8	±	25,0
12	63	3,232E-05	1,949E+06	14,10	±	0,71	1.17 ±0.22	270,8	±	36,7
13	187	5,374E-05	3,480E+06	19,03	±	0,77	1.43 ±0.25	355,9	±	29,7
14	134	3,405E-05	3,935E+06	19,72	±	0,65	1.33 ±0.25	387,4	±	35,8
15	239	5,302E-05	4,507E+06	20,96	±	0,83	1.50 ±0.28	416,6	±	31,6
16	126	2,996E-05	4,206E+06	17,85	±	0,76	1.42 ±0.24	455,1	±	44,9
17	154	5,119E-05	3,008E+06	19,51	±	0,79	1.36 ±0.25	301,4	±	27,2
18	123	3,992E-05	3,081E+06	18,01	±	0,64	1.27 ±0.22	333,6	±	32,3
19	199	5,306E-05	3,751E+06	24,45	±	0,79	1.50 ±0.28	299,9	±	23,4
20	258	8,594E-05	3,002E+06	14,55	±	0,62	1.32 ±0.20	400,2	±	30,2
21	216	4,500E-05	4,800E+06	18,70	±	1,00	1.42 ±0.22	494,2	±	42,8
22	87	3,381E-05	2,573E+06	19,30	±	1,00	1.28 ±0.29	261,4	±	31,1
23	208	5,266E-05	3,950E+06	19,88	±	0,86	1.39 ±0.22	385,8	±	31,5
	4270	1,164E-03	3,665E+06	19,94	±	3.80^a	1.37 ± 0.08^a			

^{a} Standard deviation of mean

χ^2 = 24.34 (22 degrees of freedom)

$P(\chi^2)$ = 32.98 %

Dispersion = 12 %

Pooled Age =	**359,0**	± **12.1 Ma**
Central Age =	**358,6**	± **11.4 Ma**

TRACK LENGTH DATA - 393

No.	Track length (microns)	Angle to c-axis
1	13,57	53,84
2	7,73	39,69
3	11,73	54,95
4	12,76	89,52
5	11,97	63,30
6	10,12	67,10
7	9,83	19,06
8	11,31	80,32
9	13,41	78,53
10	13,63	59,37
11	12,40	74,16
12	12,31	68,57
13	13,55	74,02
14	11,94	75,54
15	13,68	52,05
16	11,77	71,97
17	12,80	68,47
18	12,10	42,64
19	13,66	51,42
20	12,20	36,92
21	12,55	47,79
22	14,22	78,49
23	12,74	85,51
24	14,96	80,63
25	14,06	61,84
26	10,16	48,92
27	11,46	83,63
28	10,57	70,13
29	13,54	81,04
30	14,65	51,38
31	12,53	74,40
32	14,23	68,53
33	8,32	85,53
34	8,13	51,84
35	10,14	70,62
36	11,11	65,49
37	13,02	69,15

38	8,64	69,91
39	12,91	70,28
40	12,87	50,80
41	13,58	54,86
42	9,69	75,52
43	14,56	64,62
44	12,14	42,74
45	13,43	82,44
46	13,94	59,32
47	13,25	72,47
48	11,97	67,78
49	12,32	53,66
50	13,56	62,74
51	12,58	81,85
52	7,45	66,55
53	11,95	74,08
54	12,48	57,84
55	10,42	71,29
56	10,81	63,81
57	12,46	63,15
58	12,97	53,36
59	13,98	70,64
60	9,24	36,95
61	12,73	62,62
62	12,72	74,40
63	10,43	84,85
64	10,88	48,10
65	14,10	71,62
66	12,52	49,10
67	9,51	48,18
68	9,93	55,37
69	12,68	64,33
70	14,57	73,49
71	13,13	73,12
72	13,26	82,30
73	9,27	65,65
74	12,53	59,55
75	11,89	63,33
76	12,67	74,48
77	12,24	75,40
78	6,96	76,83
79	7,96	73,10
80	13,70	68,90
81	11,42	71,88
82	14,50	50,39
83	11,06	70,66
84	12,37	50,14
85	12,50	74,00
86	13,57	63,70
87	12,89	31,42
88	9,90	36,97
89	10,86	70,95
90	12,20	65,15
91	10,14	76,32
92	8,66	80,70
93	10,78	73,74
94	10,80	72,57
95	10,67	58,01
96	13,93	56,76
97	13,57	74,94
98	9,00	75,73
99	15,32	71,27
100	11,79	63,38
101	11,68	61,19

Sample:	395									

Rock Type:
Longitude/Latitude:
Calibration X/Y (μm/px):   0.0873/0.0873
Date analysed: 15-avr-2016

Mineral: Apatite
Elevation (m):
^{238}U Standard: NIST612
Software: FastTracks v2.17.16

No.	N$_S$	Area (cm^2)	ρ$_S$ (cm^{-2})	^{238}U (ppm)	±	1σ	Dpar	Age (Ma)	±	1σ
1	38	2,192E-05	1,734E+06	10,49	±	0,45	1.31 ±0.16	322,6	±	54,1
2	177	2,927E-05	6,048E+06	40,60	±	1,30	1.63 ±0.24	291,4	±	23,8
3	109	2,444E-05	4,461E+06	23,10	±	1,00	1.58 ±0.27	375,3	±	39,5
4	220	6,230E-05	3,531E+06	22,90	±	1,10	1.38 ±0.21	301,4	±	25,0
5	155	3,956E-05	3,918E+06	24,50	±	1,10	1.53 ±0.22	312,3	±	28,7
6	138	5,338E-05	2,585E+06	12,84	±	0,58	1.54 ±0.21	390,8	±	37,7
7	144	7,620E-05	1,890E+06	13,67	±	0,64	1.35 ±0.21	270,9	±	25,9
8	81	2,115E-05	3,829E+06	17,54	±	0,80	1.54 ±0.24	422,7	±	50,8
9	57	2,113E-05	2,698E+06	13,22	±	0,77	1.44 ±0.29	396,0	±	57,3
10	111	4,252E-05	2,611E+06	11,84	±	0,52	1.35 ±0.22	426,9	±	44,6
11	56	2,916E-05	1,920E+06	16,26	±	0,71	1.35 ±0.22	232,1	±	32,6
12	137	7,593E-05	1,804E+06	14,03	±	0,53	1.25 ±0.22	252,3	±	23,6
13	71	2,763E-05	2,569E+06	16,24	±	0,66	1.36 ±0.28	309,0	±	38,8
14	96	3,258E-05	2,947E+06	17,19	±	0,79	1.44 ±0.30	334,3	±	37,4
	1590	5,572E-04	3,039E+06	18,17	±	7.79[a]	1.43 ± 0.11[a]			

[a] Standard deviation of mean

χ^2 = 14.72 (13 degrees of freedom)
$P(\chi^2)$ = 32.5 %
Dispersion = 14 %

Pooled Age = **316,5** ± **16.7 Ma**
Central Age = **324,8** ± **15.6 Ma**

TRACK LENGTH DATA - 395

No.	Track length (microns)	Angle to c-axis
1	8,82	58,91
2	9,83	51,29
3	12,04	58,88
4	8,85	81,48
5	12,48	64,55
6	13,13	35,90
7	11,94	71,94
8	9,55	81,94
9	9,57	52,58
10	11,72	77,01
11	11,66	70,31
12	9,66	60,88
13	14,96	70,99
14	15,30	63,71
15	13,08	44,44
16	12,66	59,04
17	13,71	58,37
18	11,38	77,86
19	11,43	76,07
20	10,44	71,86
21	9,73	83,88
22	8,92	71,76
23	11,20	62,78
24	13,77	41,43
25	10,42	68,33
26	11,37	66,14
27	14,41	63,70
28	12,36	57,62
29	10,69	61,44
30	9,28	66,82
31	8,12	81,11
32	12,22	73,84
33	14,88	82,30
34	17,57	52,54
35	11,10	52,90
36	13,14	61,26
37	11,87	78,72
38	12,12	62,80
39	12,82	49,38
40	11,74	42,91
41	9,79	53,71
42	13,31	61,22
43	14,47	71,64
44	11,16	51,44
45	13,00	38,19
46	12,61	53,45
47	12,18	75,44
48	9,78	56,96
49	9,81	71,37

50	12,81	74,08
51	12,69	53,00
52	13,03	70,55
53	12,00	29,03
54	13,04	61,77
55	12,63	68,80
56	14,39	50,39
57	11,57	30,62
58	14,20	38,88
59	10,34	58,91
60	11,82	62,25
61	11,85	42,37
62	13,24	68,48
63	11,13	68,54
64	11,38	65,54
65	7,92	78,87
66	10,12	60,83
67	9,24	58,53
68	9,49	76,98
69	11,41	76,64
70	12,53	63,40
71	9,71	46,43
72	13,12	74,11
73	8,35	69,05
74	14,35	78,77
75	11,64	74,53
76	14,65	76,03
77	12,06	86,25
78	11,56	72,46
79	12,77	70,71
80	11,27	82,94
81	14,49	59,95
82	10,36	52,88
83	13,41	41,83
84	8,63	70,92
85	12,45	77,75
86	12,97	42,88
87	11,59	50,45
88	15,17	72,15
89	12,48	49,94
90	11,73	74,44
91	13,93	58,14
92	13,14	73,51
93	11,22	79,33
94	11,21	76,22
95	9,93	39,51
96	8,99	52,45
97	11,96	62,41
98	10,55	75,33
99	11,63	66,14
100	13,54	41,21

Sample: 23-01

Rock Type:						Mineral:		Apatite		
Longitude/Latitude:						Elevation (m):				
Calibration X/Y (µm/px):		0.0873/0.0873				^{238}U Standard:		NIST612		
Date analysed:		10-mai-2016				Software:		FastTracks v2.17.19		

No.	N_S	Area (cm^2)	ρs (cm^{-2})	^{238}U (ppm)	±	1σ	Dpar	Age (Ma)	±	1σ
1	117	1,264E-04	9,257E+05	4,82	±	0,30	1.75 ±0.18	373,3	±	41,6
2	86	6,536E-05	1,316E+06	3,40	±	0,19	1.63 ±0.16	731,5	±	88,8
3	119	9,711E-05	1,225E+06	3,52	±	0,19	1.63 ±0.13	661,3	±	70,4
4	68	5,325E-05	1,277E+06	5,82	±	0,25	1.65 ±0.24	424,8	±	54,6
5	55	8,134E-05	6,762E+05	3,75	±	0,22	1.41 ±0.23	351,1	±	51,6
6	48	2,945E-05	1,630E+06	4,38	±	0,24	1.42 ±0.18	704,8	±	108,8
7	51	6,856E-05	7,439E+05	3,49	±	0,22	1.57 ±0.23	413,0	±	63,4
8	101	3,954E-05	2,554E+06	11,78	±	0,66	1.59 ±0.26	419,9	±	47,9
9	159	1,045E-04	1,522E+06	9,12	±	0,48	2.06 ±0.37	325,6	±	31,0
10	75	7,707E-05	9,732E+05	3,13	±	0,18	1.82 ±0.41	594,0	±	76,6
11	60	5,509E-05	1,089E+06	4,45	±	0,24	1.66 ±0.28	472,0	±	66,0
12	168	1,206E-04	1,393E+06	6,93	±	0,28	1.44 ±0.24	390,2	±	34,0
13	149	5,913E-05	2,520E+06	10,70	±	0,48	1.57 ±0.29	454,9	±	42,5
14	52	3,784E-05	1,374E+06	3,70	±	0,26	1.75 ±0.24	703,3	±	109,3
15	161	8,311E-05	1,937E+06	7,21	±	0,38	1.70 ±0.31	516,4	±	49,0
16	55	6,943E-05	7,922E+05	3,37	±	0,22	1.63 ±0.19	454,1	±	68,0
17	192	1,512E-04	1,269E+06	5,22	±	0,32	1.84 ±0.38	469,0	±	44,4
18	116	7,959E-05	1,458E+06	4,37	±	0,25	1.87 ±0.26	635,3	±	69,3
19	89	4,186E-05	2,126E+06	8,90	±	0,47	1.68 ±0.25	461,1	±	54,6
	1921	1,440E-03	1,411E+06	5,69	±	2.67[a]	1.67 ±0.16[a]			

[a] Standard deviation of mean

χ^2 = 20.4 (18 degrees of freedom)
P(χ^2) = 31.05 %
Dispersion = 21 %

Pooled Age = **462,7** ± **29.9 Ma**
Central Age = **485,5** ± **26.7 Ma**

TRACK LENGTH DATA – 23-01

No.	Track length (microns)	Angle to c-axis
1	9,62	46,91
2	12,15	51,67
3	12,56	42,19
4	12,47	57,65
5	14,12	60,80
6	12,22	74,56
7	14,46	50,80
8	12,86	70,62
9	12,85	72,88
10	11,77	79,39
11	9,84	44,68
12	14,06	66,72
13	10,89	80,47
14	10,77	48,87
15	10,42	59,85
16	9,54	60,07
17	10,70	33,40
18	13,19	81,16
19	10,83	79,26
20	10,09	62,31
21	11,57	50,92
22	13,58	78,69
23	11,22	59,64
24	10,06	62,66
25	13,77	82,29
26	12,40	48,45
27	7,93	75,89
28	13,71	86,92
29	14,23	36,75
30	11,17	38,81
31	10,89	53,32
32	13,27	60,05
33	10,81	37,98
34	10,66	68,02
35	9,25	59,84
36	13,87	34,50
37	12,28	39,79
38	11,51	47,89
39	13,29	35,26
40	13,86	54,33
41	13,42	38,39
42	11,77	70,28

43	14,62	72,36
44	14,38	45,85
45	10,74	62,77
46	8,57	64,05
47	10,53	53,32
48	12,00	71,44
49	14,05	68,44
50	9,74	65,91
51	13,82	42,65
52	13,10	29,89
53	10,41	52,98
54	11,94	74,00
55	12,27	68,23
56	11,92	39,16
57	14,22	53,30
58	13,97	61,59
59	13,84	74,14
60	13,58	62,46
61	13,66	32,32
62	13,69	69,20
63	12,62	81,74
64	13,26	72,16
65	13,31	74,75
66	13,38	53,63
67	10,55	53,03
68	10,43	47,00
69	9,68	67,91
70	10,82	67,22
71	13,25	78,15
72	12,46	51,84
73	13,79	79,96
74	14,37	41,74
75	12,97	51,79
76	14,25	54,86
77	13,42	37,33
78	10,89	76,38
79	12,68	68,42
80	10,25	52,59
81	13,21	65,34
82	12,35	84,51
83	13,15	76,34
84	11,06	75,22
85	11,14	72,24
86	13,27	72,34
87	14,31	72,65
88	11,49	29,45
89	11,79	83,07
90	13,87	66,01
91	12,68	74,72
92	8,70	63,51
93	10,64	64,74
94	12,43	77,19
95	14,32	45,81
96	10,55	56,22
97	11,48	57,71
98	13,05	69,98
99	11,16	42,08
100	14,06	64,28

Sample: 21-01L

Rock Type:							Mineral:		Apatite	
Longitude/Latitude:							Elevation (m):			
Calibration X/Y (µm/px):		0.0873/0.0873					[238]U Standard:		NIST612	
Date analysed:		14-avr-2016					Software:		FastTracks v2.17.16	

No.	N_S	Area (cm²)	ρ_S (cm⁻²)	[238]U (ppm)	±	1σ	Dpar	Age (Ma)	±	1σ
1	73	5,628E-05	1,297E+06	4,29	±	0,25	1.53 ±0.18	578,3	±	75,6
2	45	2,233E-05	2,015E+06	8,68	±	0,53	1.83 ±0.24	448,6	±	72,3
3	199	2,079E-05	9,574E+06	41,20	±	1,70	1.66 ±0.21	449,0	±	36,8
4	45	1,031E-05	4,366E+06	24,20	±	1,00	1.45 ±0.23	351,3	±	54,3
5	122	3,363E-05	3,628E+06	11,78	±	0,57	1.67 ±0.29	588,6	±	60,4
6	83	1,389E-05	5,977E+06	45,70	±	3,10	1.58 ±0.25	256,6	±	33,1
7	31	1,843E-05	1,682E+06	8,90	±	0,43	1.52 ±0.30	367,5	±	68,4
8	65	2,577E-05	2,522E+06	15,03	±	0,84	1.86 ±0.30	327,3	±	44,5
9	29	2,528E-05	1,147E+06	5,96	±	0,32	1.38 ±0.24	374,1	±	72,3
10	61	2,093E-05	2,915E+06	19,12	±	0,85	1.21 ±0.16	298,1	±	40,4
11	172	3,767E-05	4,566E+06	20,27	±	0,91	1.52 ±0.27	435,7	±	38,6
12	70	2,752E-05	2,543E+06	13,62	±	0,61	1.79 ±0.25	363,2	±	46,4
13	118	4,924E-05	2,396E+06	13,30	±	0,55	1.63 ±0.31	350,8	±	35,4
14	52	3,561E-05	1,460E+06	7,53	±	0,42	1.39 ±0.26	376,8	±	56,3
15	64	2,546E-05	2,514E+06	11,74	±	0,60	1.39 ±0.26	414,9	±	56,0
	1229	4,231E-04	3,240E+06	16,75	±	12.15[a]	1.56 ± 0.18[a]			

[a] Standard deviation of mean

χ^2 = 14.08 (14 degrees of freedom)

$P(\chi^2)$ = 44.4 %

Dispersion = 18 %

Pooled Age = **395,2** ± **24.5 Ma**

Central Age = **393,0** ± **23.0 Ma**

TRACK LENGTH DATA – 21-01L

No.	Track length (microns)	Angle to c-axis
1	14,31	65,51
2	11,09	73,78
3	13,12	58,20
4	13,44	59,51
5	10,89	69,80
6	10,22	56,56
7	14,22	70,79
8	14,59	61,57
9	11,81	74,98
10	11,31	72,15
11	10,39	74,02
12	12,76	72,29
13	10,34	73,78
14	12,95	52,19
15	13,29	80,43
16	11,34	76,46
17	10,99	81,70
18	9,84	88,06
19	13,61	56,27
20	11,00	73,19
21	15,01	80,54
22	13,13	37,36
23	9,22	81,56
24	11,01	78,13
25	13,14	76,88
26	11,37	86,50
27	10,69	73,63
28	11,99	59,79
29	14,81	75,37
30	11,66	59,23
31	9,86	25,09
32	12,72	22,14
33	10,77	26,42
34	12,99	37,56
35	10,92	51,32
36	13,76	64,38
37	13,69	65,86
38	13,43	25,70
39	14,60	50,59
40	11,70	76,02
41	9,07	72,84
42	10,57	36,99
43	14,65	53,33
44	15,53	72,63
45	14,28	71,62
46	13,85	0,00
47	12,74	30,06
48	12,03	59,66

49	13,73	64,71
50	12,49	70,76
51	13,72	83,01

Sample: LKA-15

Rock Type:						Mineral:		Apatite	
Longitude/Latitude:						Elevation (m):			
Calibration X/Y (µm/px):		0.0873/0.0873				[238]U Standard:		NIST612	
Date analysed:		05-mai-2016				Software:		FastTracks v2.17.14	

No.	N_S	Area (cm²)	ρ_S (cm⁻²)	[238]U (ppm)	±	1σ	Dpar	Age (Ma)	±	1σ
1	62	7,582E-05	8,177E+05	5,26	±	0,31	1.44 ±0.36	303,8	±	42,5
2	58	6,607E-05	8,779E+05	6,05	±	0,32	1.37 ±0.33	284,0	±	40,2
3	373	1,100E-04	3,391E+06	25,44	±	0,92	1.49 ±0.24	261,4	±	16,5
4	75	5,459E-05	1,374E+06	14,78	±	0,64	1.54 ±0.36	183,4	±	22,6
5	320	8,362E-05	3,827E+06	47,20	±	2,10	1.32 ±0.24	160,3	±	11,4
6	80	1,488E-04	5,377E+05	5,57	±	0,29	1.36 ±0.25	190,3	±	23,5
7	30	4,738E-05	6,332E+05	5,67	±	0,30	1.36 ±0.25	219,7	±	41,8
8	22	3,865E-05	5,693E+05	3,30	±	0,20	1.33 ±0.14	336,3	±	74,5
9	8	5,965E-05	1,341E+05	1,49	±	0,12	1,45	177,6	±	64,4
10	15	6,302E-05	2,380E+05	1,27	±	0,11	1.15 ±0.21	364,5	±	99,3
11	26	2,269E-05	1,146E+06	8,01	±	0,51	1.43 ±0.26	280,1	±	57,8
12	36	3,817E-05	9,431E+05	8,27	±	0,40	1.86 ±0.07	224,3	±	38,9
13	76	3,118E-05	2,438E+06	21,42	±	0,88	1.36 ±0.26	223,8	±	27,3
14	40	6,961E-05	5,746E+05	5,54	±	0,30	1.50 ±0.54	204,3	±	34,1
15	180	9,590E-05	1,877E+06	15,88	±	0,66	1.31 ±0.28	232,3	±	19,8
	1401	1,005E-03	1,292E+06	11,68	±	12.14[a]	1.42 ±0.16[a]			

[a] Standard deviation of mean

χ^2 = 19.82 (14 degrees of freedom)

$P(\chi^2)$ = 13.58 %

Dispersion = 17 %

Pooled Age	=	**215,1**	±	**15.0 Ma**
Central Age	=	**230,6**	±	**13.5 Ma**

TRACK LENGTH DATA – LKA-15

No.	Track length (microns)	Angle to c-axis
1	14,27	62,80
2	12,04	53,05
3	11,16	56,41
4	13,14	57,90
5	9,54	41,59
6	10,13	68,85
7	11,09	75,91
8	12,87	72,62
9	10,15	69,71
10	13,04	56,64
11	13,85	45,16
12	5,20	66,36
13	13,48	52,33
14	15,78	78,79
15	10,65	72,72
16	13,04	56,35
17	13,17	61,10
18	8,95	66,63
19	13,27	60,22
20	15,25	44,18
21	11,63	62,98
22	13,81	29,11
23	7,01	50,66
24	13,09	11,83
25	12,11	71,79
26	12,20	55,98
27	14,47	70,80
28	10,35	82,87
29	12,62	82,36
30	15,16	70,96
31	9,58	71,65
32	13,33	59,89
33	14,02	42,46
34	12,47	79,10
35	12,51	78,55
36	16,84	65,50
37	14,85	82,06
38	10,23	62,08
39	8,85	81,99
40	12,85	64,33
41	8,01	33,11
42	11,68	65,61
43	12,67	83,17
44	10,54	51,62
45	11,81	66,92
46	12,26	63,91
47	13,32	84,93
48	10,55	61,09

49	12,60	74,86
50	15,99	44,35
51	10,79	75,25